DES Y3 BAO measurements

Kwan Chuen Chan
Sun-Yat Sen University

In collaboration with Dark Energy Survey

Rencontres du Vietnam, Quy Nhon, 7 Aug 2023

Baryonic Acoustic Oscillations (BAO)

- Acoustic oscillations occur in the early universe, later imprinted in the distribution of the large-scale structure

- Standard ruler in the late universe. Can be measured in the correlation function or galaxy power spectrum of the LSS tracers

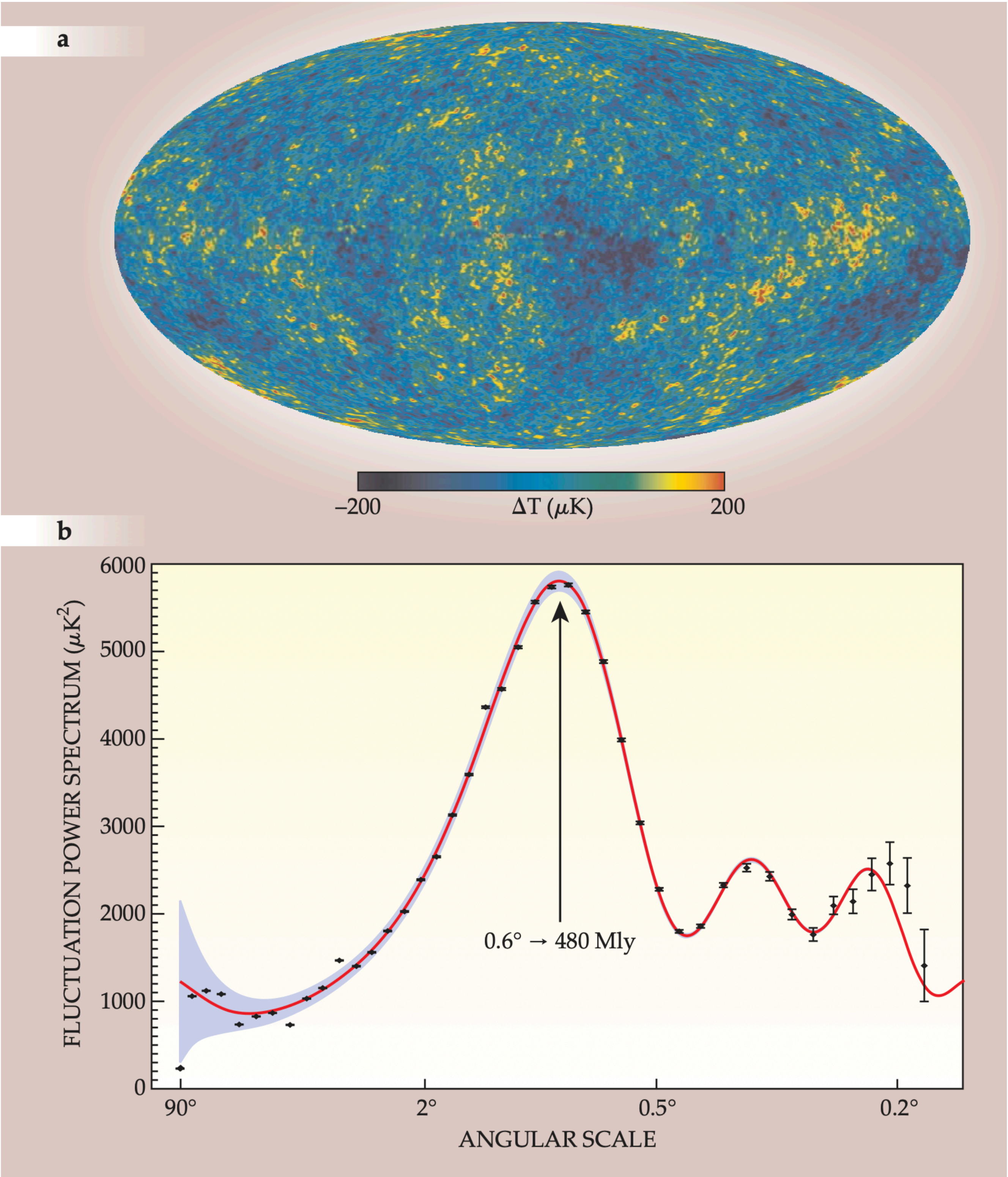

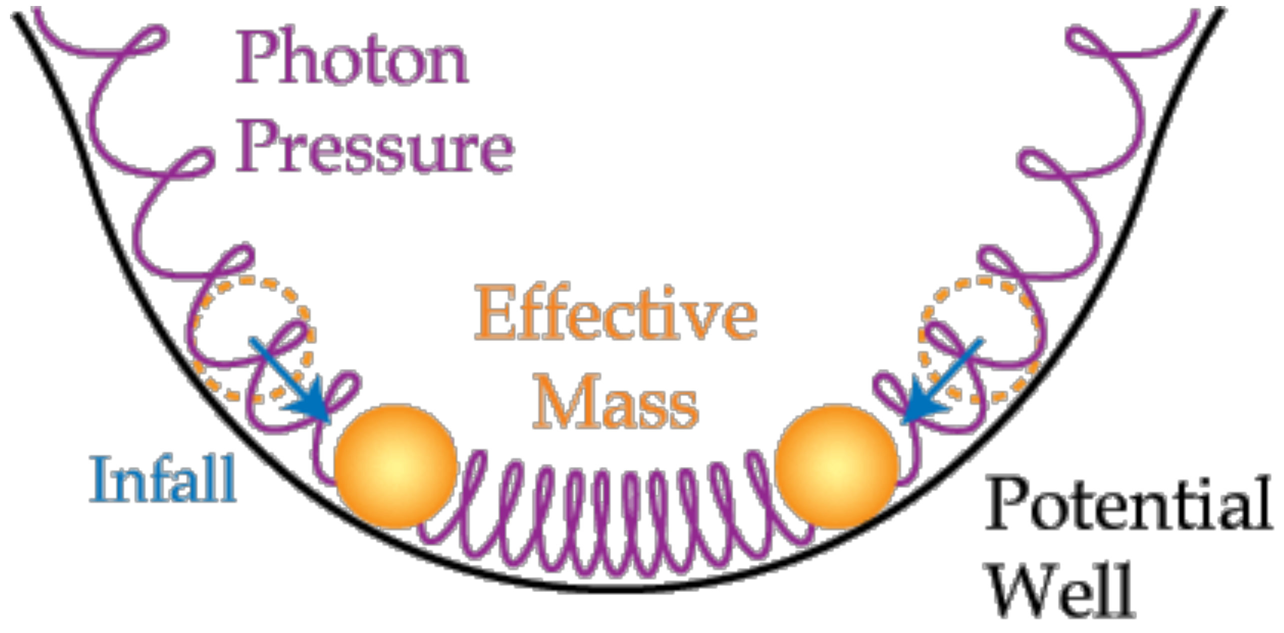

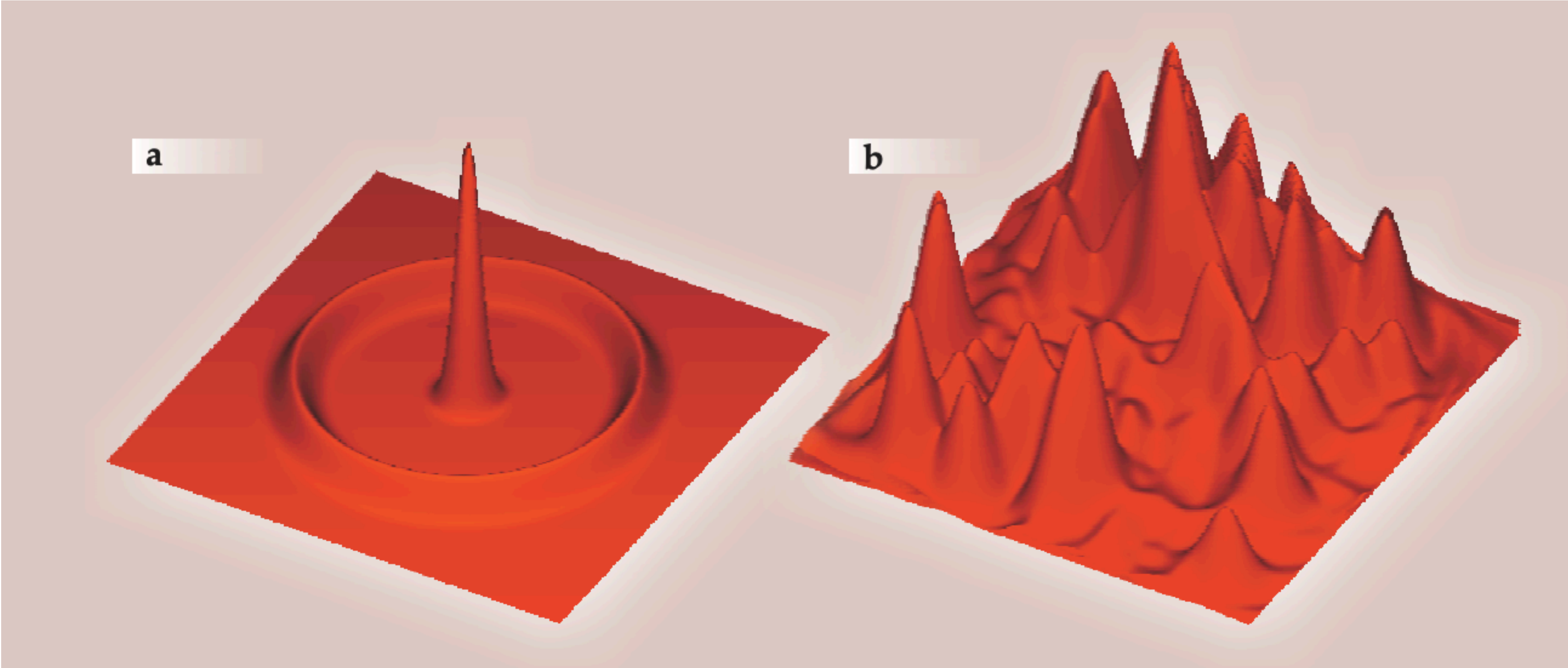

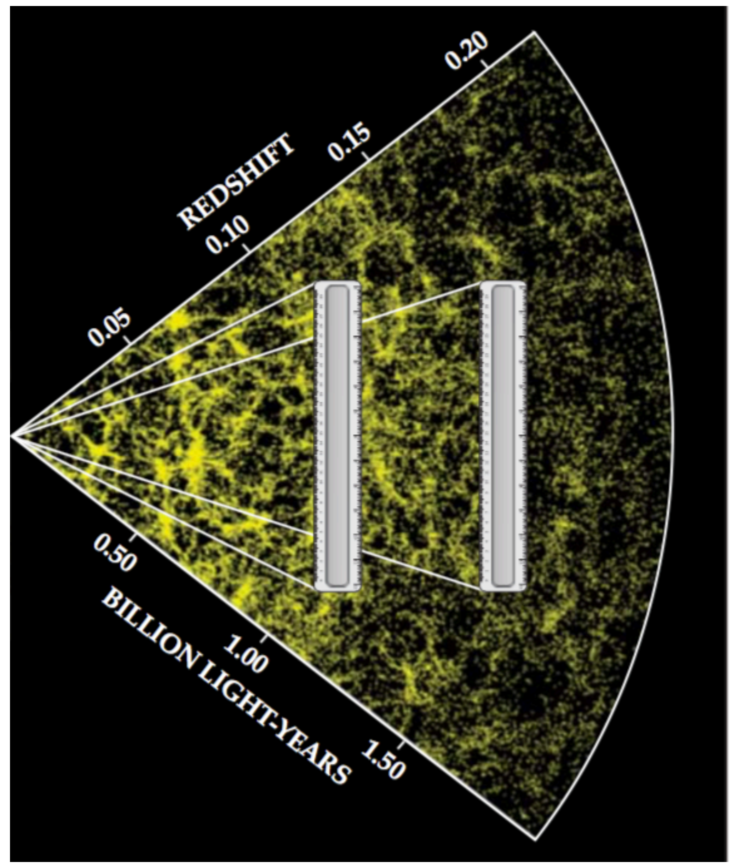

Formation of BAO

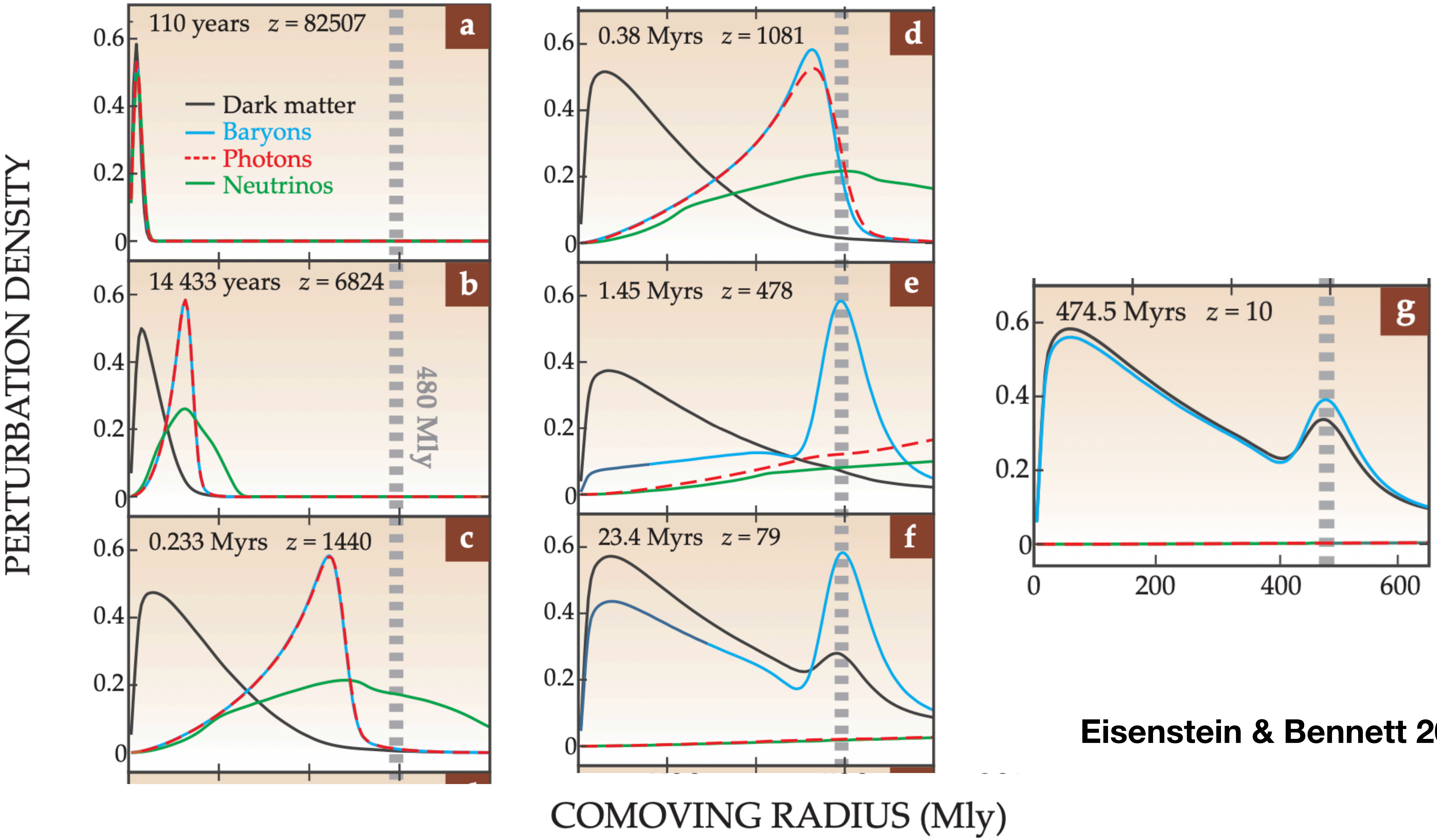

Eisenstein & Bennett 2008

The physical constraints from BAO

- Assuming given sound horizon, radial BAO probes Hubble parameter, transverse BAO constrains angular diameter distance

$$\Delta z_{\rm BAO} = \frac{r_{\rm d} H(z)}{c} \qquad \theta_{\rm BAO} = \frac{r_{\rm d}}{D_M(z)}$$

- Spec-z surveys constrain both radial and transverse BAO, photo-z surveys only probe the latter

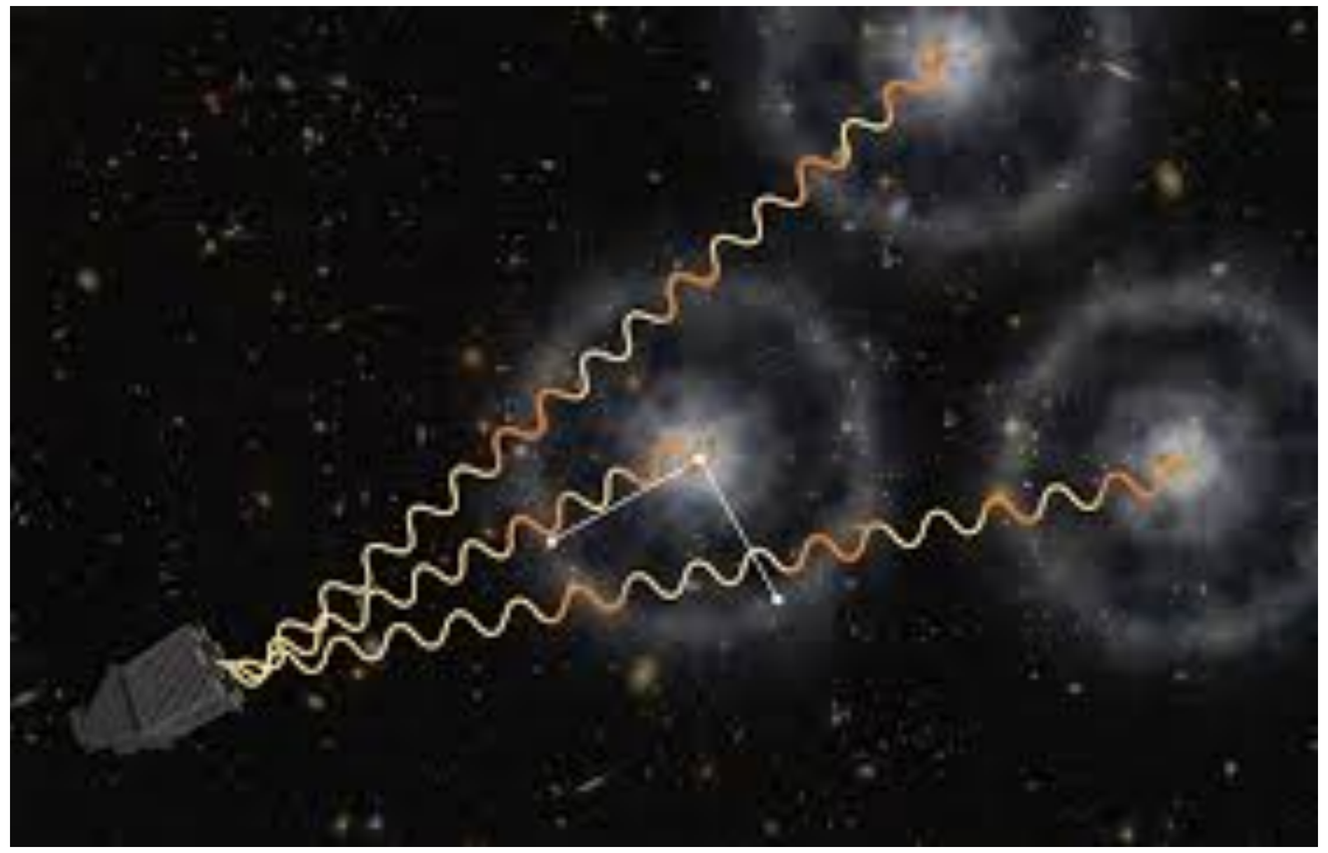

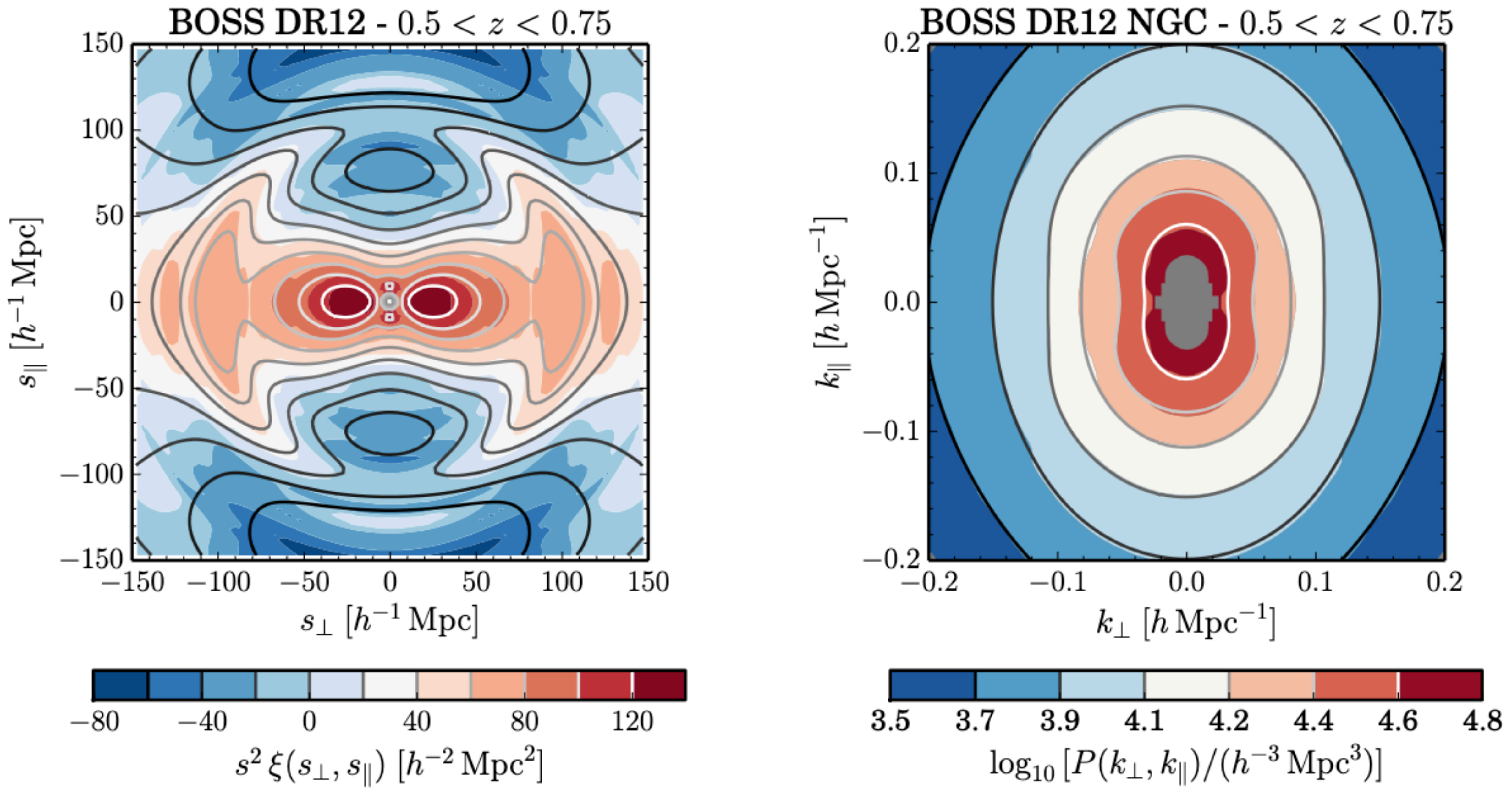

Alam +, BOSS, 2016

Dark Energy Survey Year 3

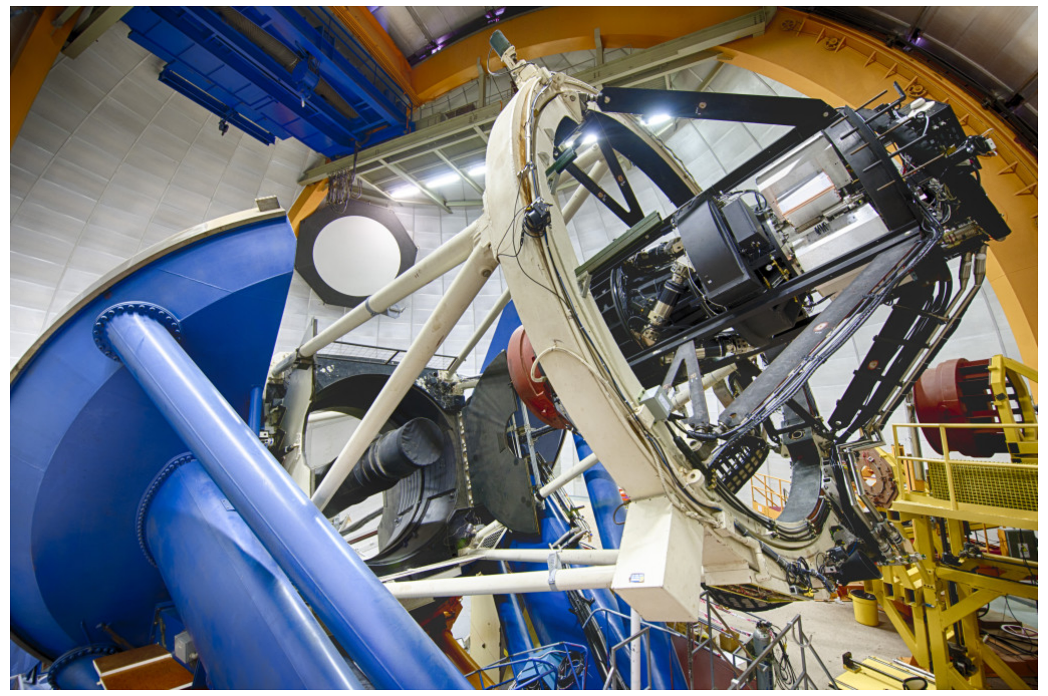

- Dark Energy Survey (DES) is an ongoing photometric survey, most well-known for weak lensing
- Blanco 4-meter telescope at Cerro Tololo Inter-American Observatory in Chile
- Dark Energy Camera, Field of view: 3 sq deg, 570-megapixels CCD
- Y3 observing time from 2013 to 2015

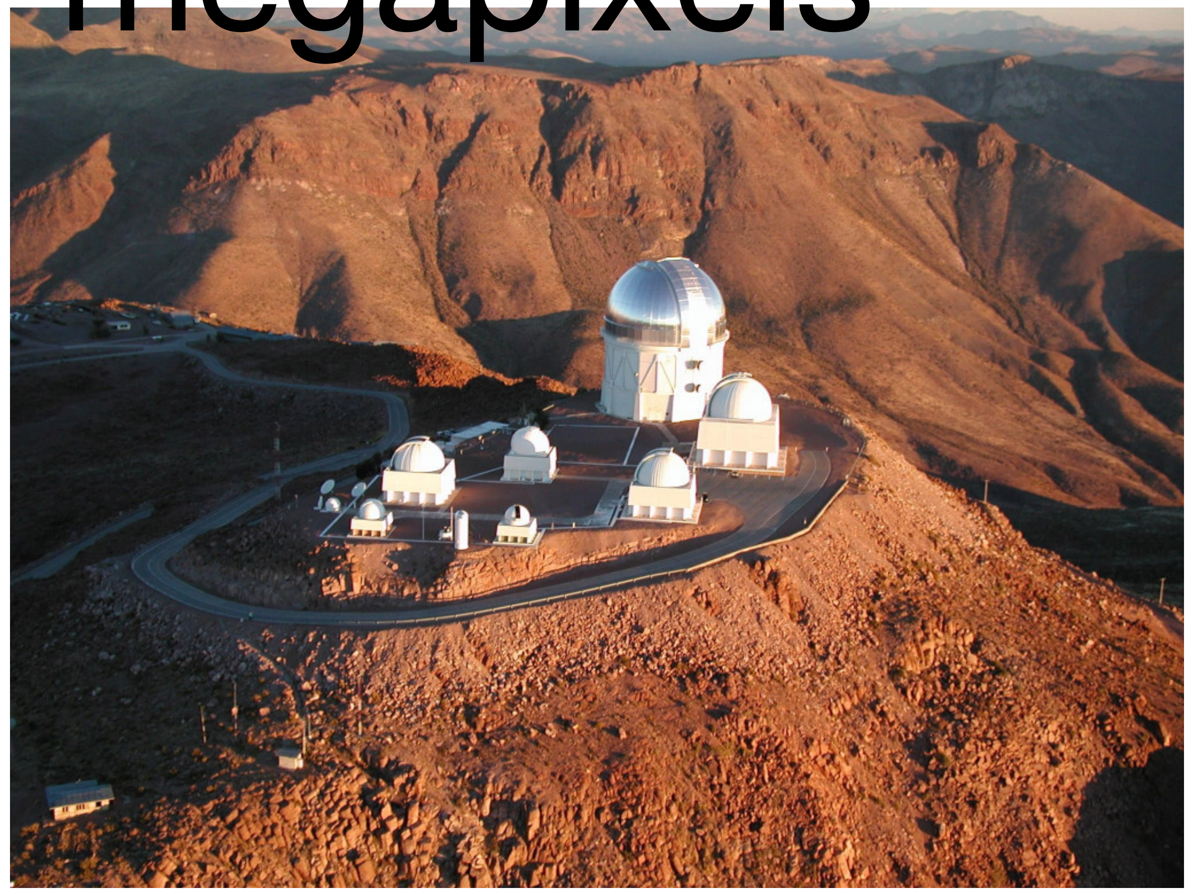

DES Y3

- DES Y3 gold sample covers about 5000 sq deg
- After masking, DES Y3 BAO sample covers about 4100 sq degree, with mean redshift of 0.83.

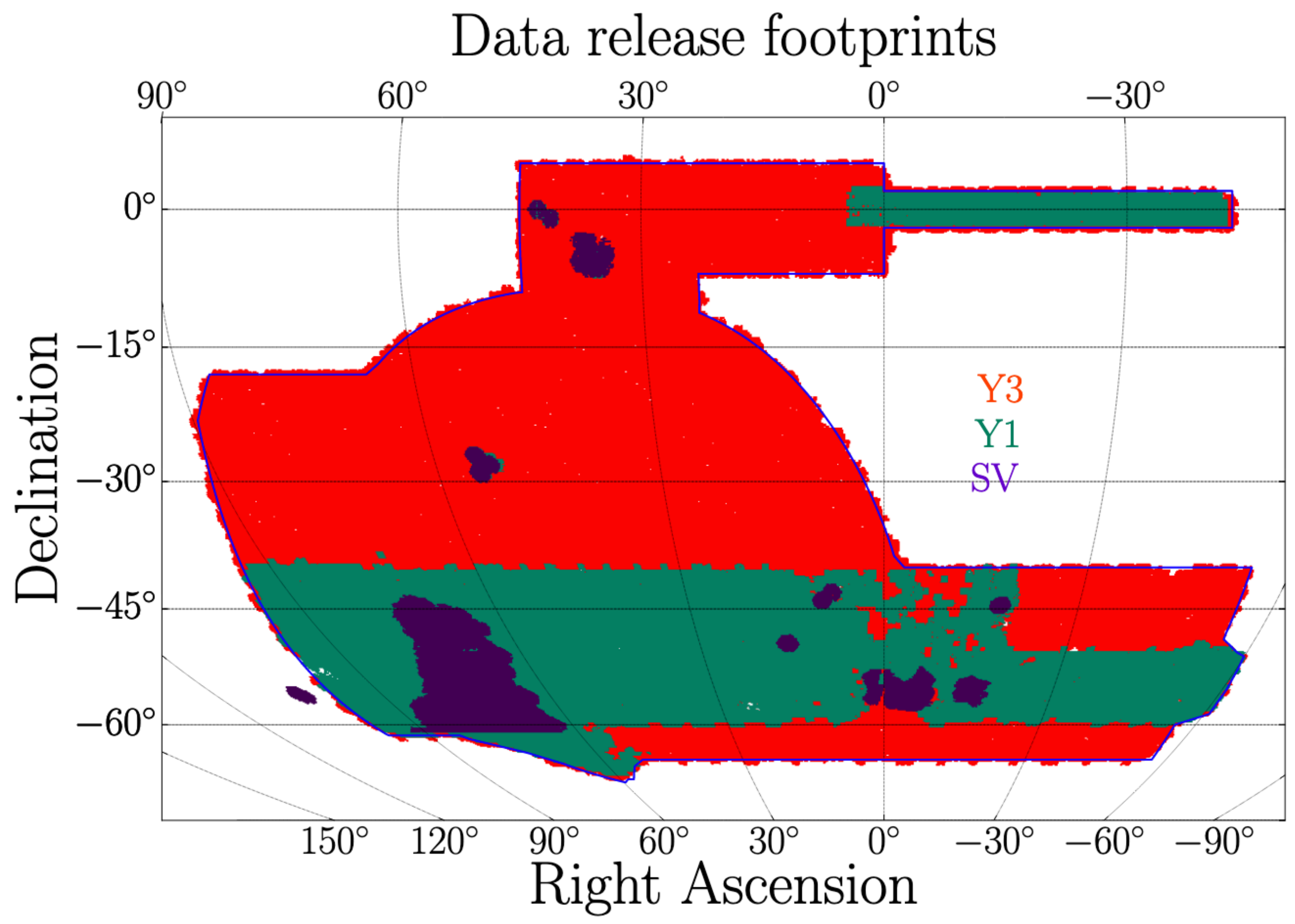

Sevilla-Noarbe +, 2011.03407

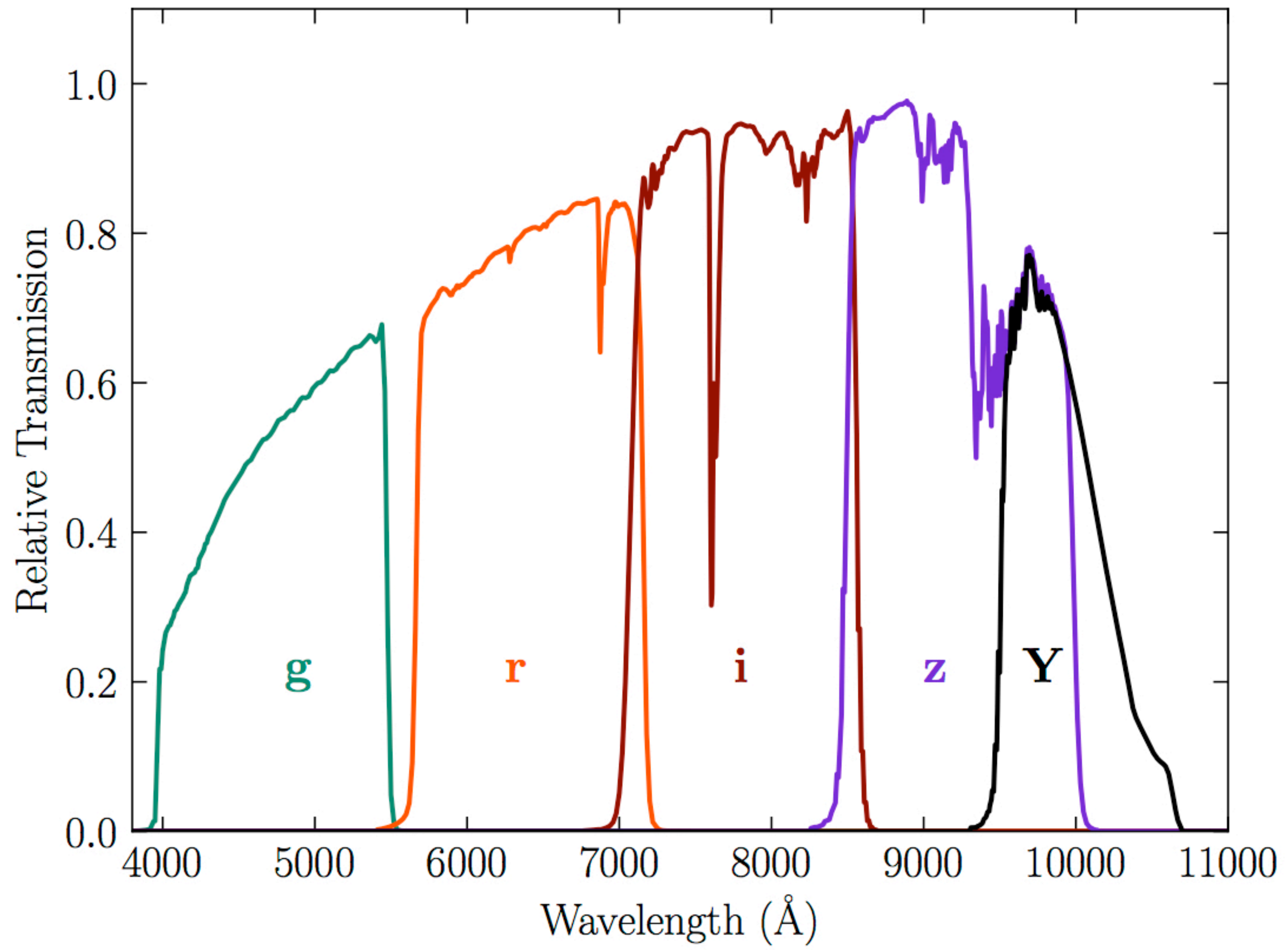

Fiducial DES Y3 BAO analysis

- 7 million red galaxies z= 0.6 to 1.1, 5 tomographic bins
- 10 σ depth of 22, 22, 22.3, and 21 for griz

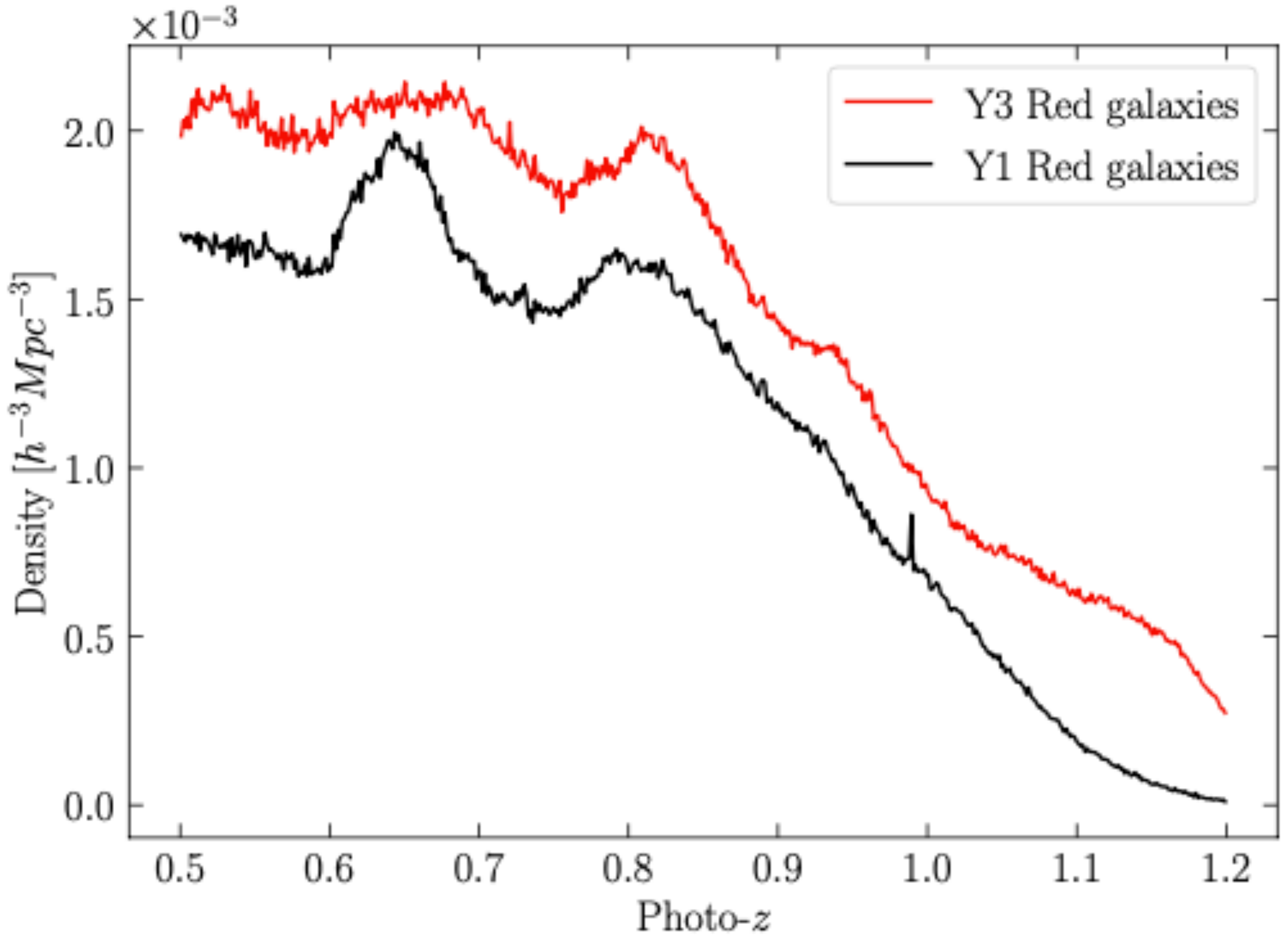

Redshift limits	$\bar{z}$	W_{68}	σ_{68}	Number of galaxies	blind galaxy bias
0.6 < z < 0.7	0.648 ± 0.003	0.0455 ± 0.003	0.021 ± 0.001	1,478,178	1.79 ± 0.09
0.7 < z < 0.8	0.742 ± 0.003	0.0522 ± 0.002	0.025 ± 0.002	1,632,805	1.83 ± 0.10
0.8 < z < 0.9	0.843 ± 0.003	0.0629 ± 0.003	0.029 ± 0.002	1,727,646	2.02 ± 0.12
0.9 < z < 1.0	0.932 ± 0.004	0.0633 ± 0.003	0.030 ± 0.003	1,315,604	2.09 ± 0.14
1.0 < z < 1.1	1.020 ± 0.006	0.0808 ± 0.006	0.040 ± 0.005	877,760	2.4 ± 0.08

Carnero Rosell +, 2107.05477

σ_{68} is the width of the distribution $|z_{\rm photo} - z_{\rm spec}|/(1 + z_{\rm spec})$ and W_{68} is the width of the $z_{\rm spec}$ in the photo-z bin.

Removing survey property dependence by systematic weight

- Data are taken over long period of time with different survey properties. Many systematic property maps are considered
- Systematic weight is applied iteratively until the galaxy density doesn't show appreciable trend w.r.t. the survey properties

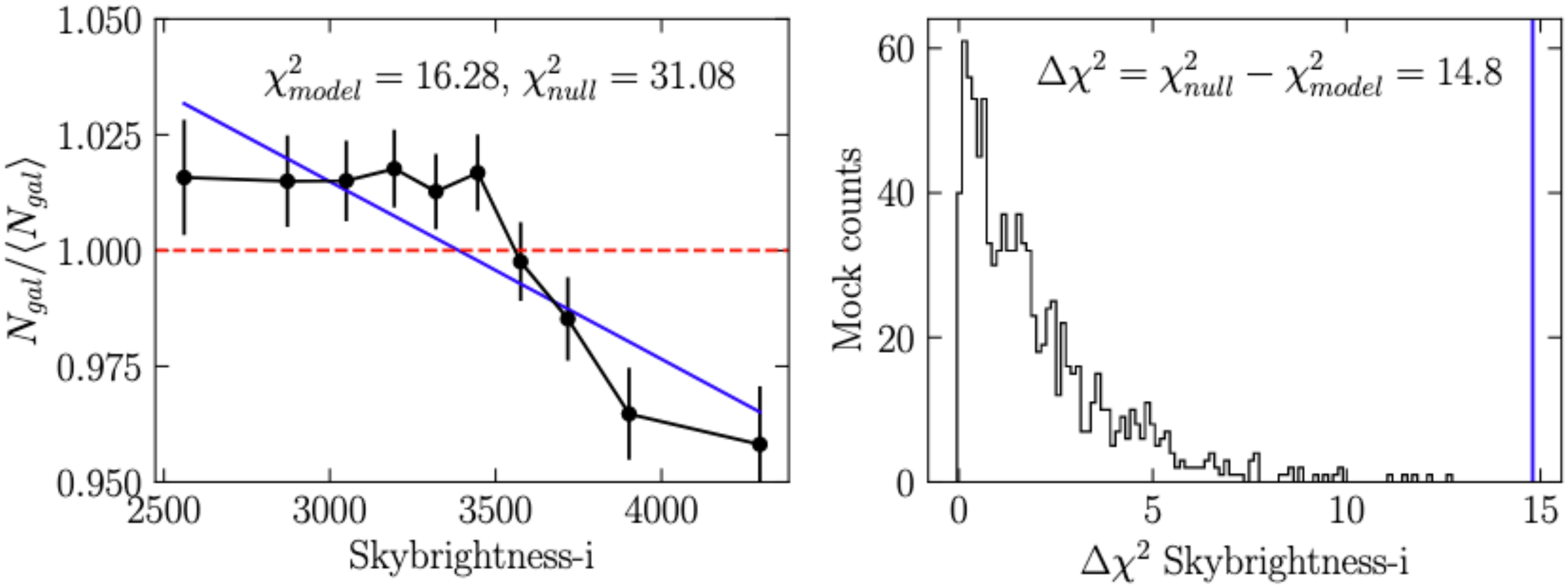

Carnero Rosell +, 2107.05477

Photo-z

- Photo-z obtained with DNF algorithm, based on kNN with improved metric and fitting to a hyperplane to the neighbors, outperform BPZ and Annz2

- Trained with spec-z catalogs like SDSS and OzDES

- Typical photo-z uncertainty is 0.03(1+z) , averaged photo-z bias is $\lesssim$0.02

Bias of the mean of the distribution, can bias the results

$$z_{\rm bias} = \frac{1}{N}\sum_{i=1}^{N}(z_{\rm photo} - z_{\rm spec})$$

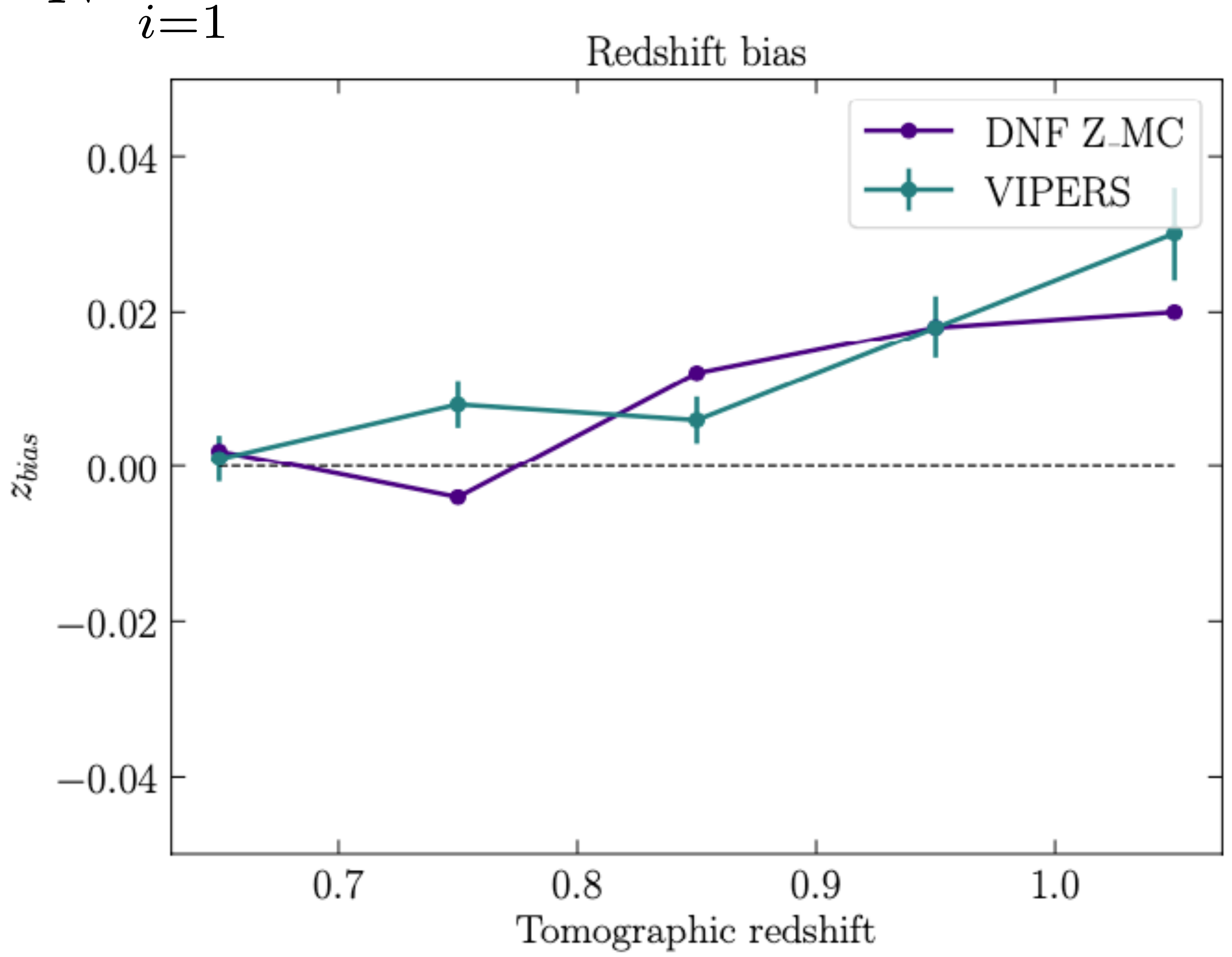

width of the photo-z distribution, can increase the error bar

$$\sigma_{68} = \frac{|z_{\rm photo} - z_{\rm spec}|}{1 + z_{\rm spec}}$$

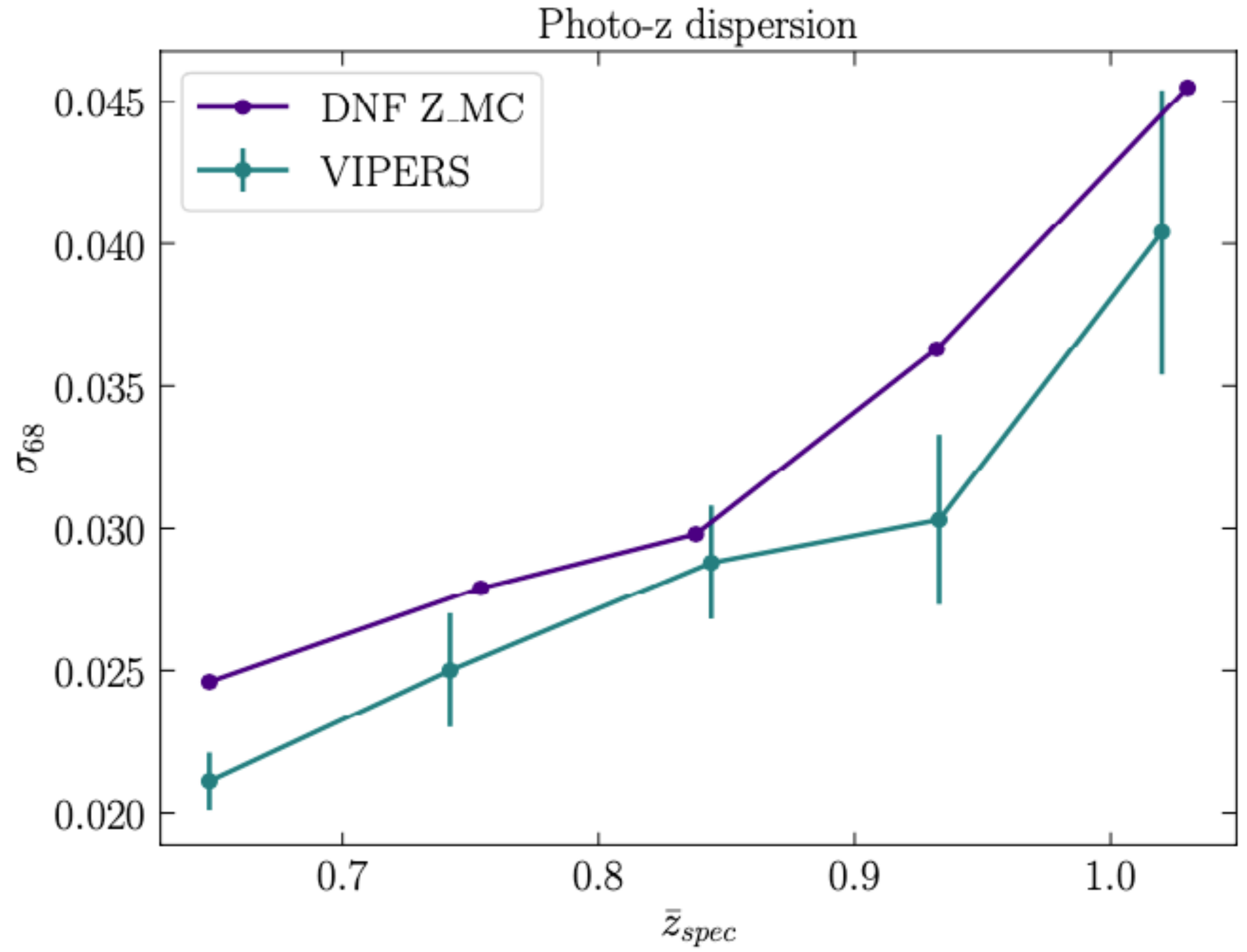

Carnero Rosell +, 2107.05477

ICE-COLA mocks

- The analysis pipeline is tested with a set of dedicated lightcone mocks
- 1952 mocks derived from 488 sets of ICE-COLA simulations.
- The photo-z distribution of the mocks matches the samples

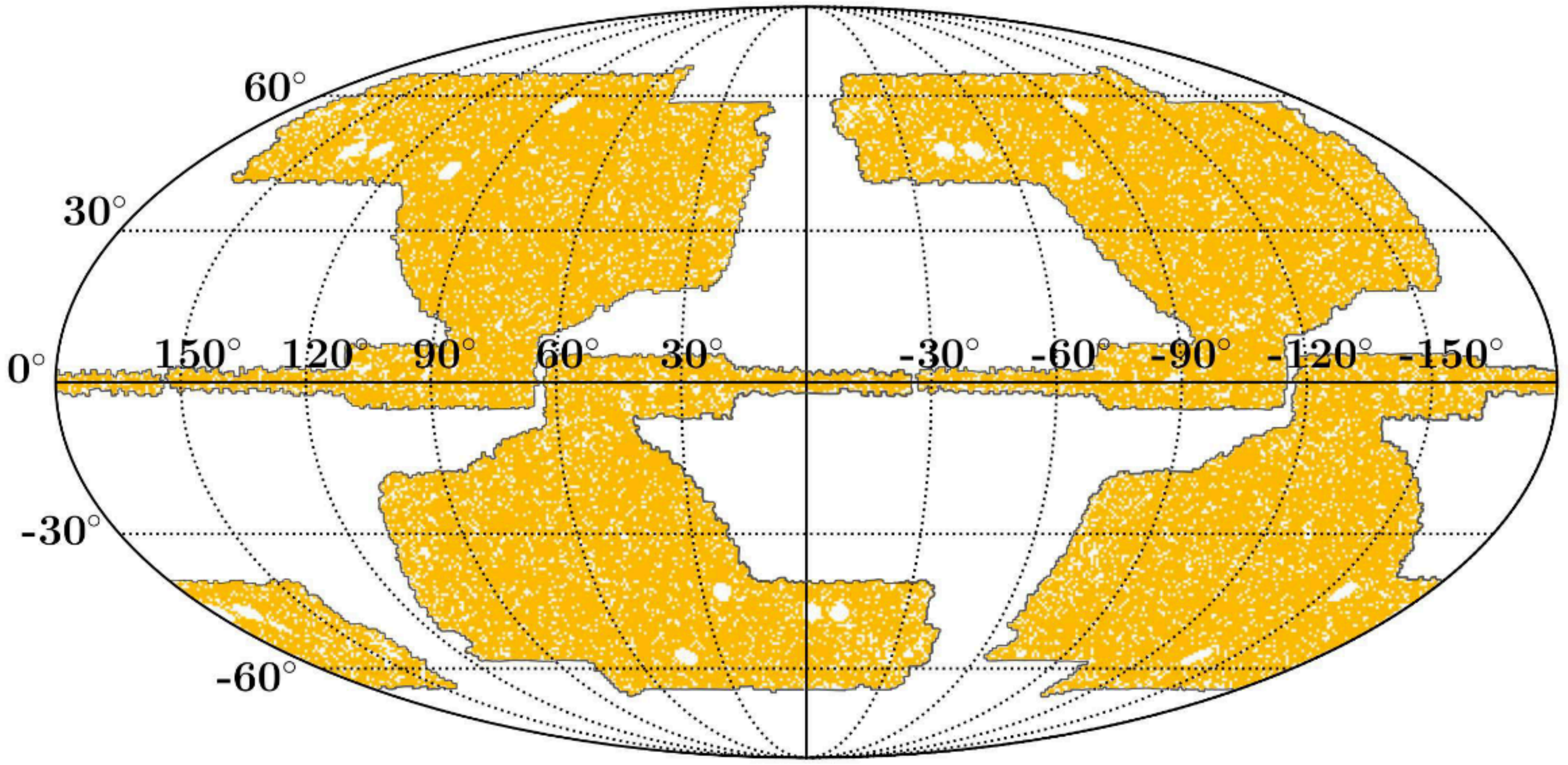

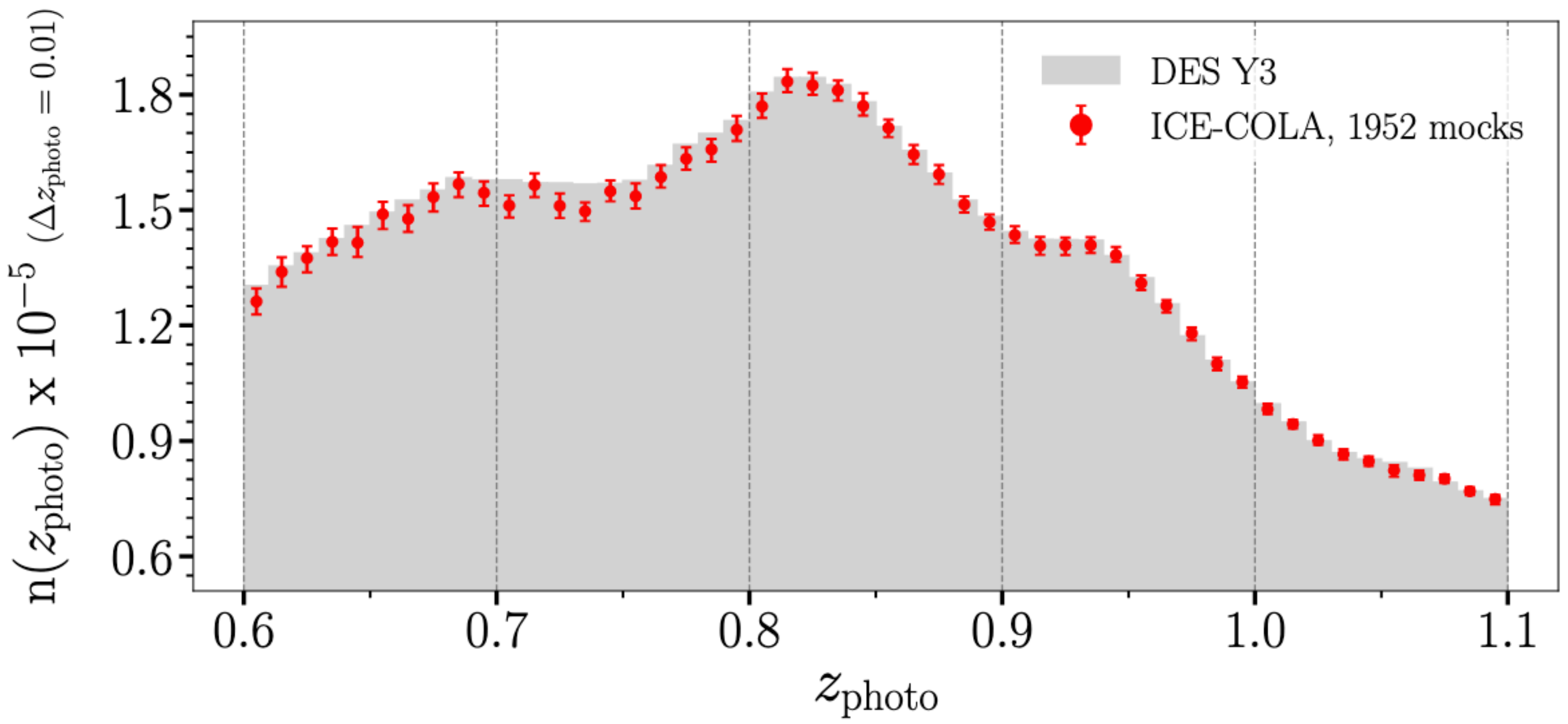

Ferrero +, 2107.04602

Angular clustering statistics

- The BAO is measured using angular correlation function w and angular power spectrum C_ℓ

$$w(\theta, z_{\rm p}, z'_{\rm p}) = \sum_\ell i^\ell \int dz \phi(z|z_{\rm p}) \int dz' \phi(z'|z'_{\rm p}) \mathcal{L}_\ell(\hat{\boldsymbol{s}} \cdot \hat{\boldsymbol{e}}) \int \frac{dk k^2}{2\pi^2} j_\ell(ks) P_\ell(k, z, z')$$

$$P(k, \mu) = (b + \mu^2 f)^2 \left[(P_{\rm lin} - P_{\rm nw}) e^{-k^2 \Sigma^2_{\rm tot}} + P_{\rm nw} \right]$$

$$C_\ell = 2\pi \int_{-1}^{1} d(\cos\theta)\, w(\theta) \mathcal{L}_\ell(\cos\theta)$$

- BAO position in w or C_ℓ is extracted by fitting the full template to the data

$$M(x) = B T_{{\rm BAO},\alpha}(x') + A(x),$$

For w, $x = \theta$, $x' = \alpha\theta$, $T = w$, $A(\theta) = \sum_i \frac{a_i}{\theta^i}$ For C_ℓ, $x = \ell$, $x' = \frac{\ell}{\alpha}$, $T = C_\ell$, $A(\ell) = \sum_i a_i \ell^i$.

Angular BAO measurements

- w and C_ℓ results are consistent with each other

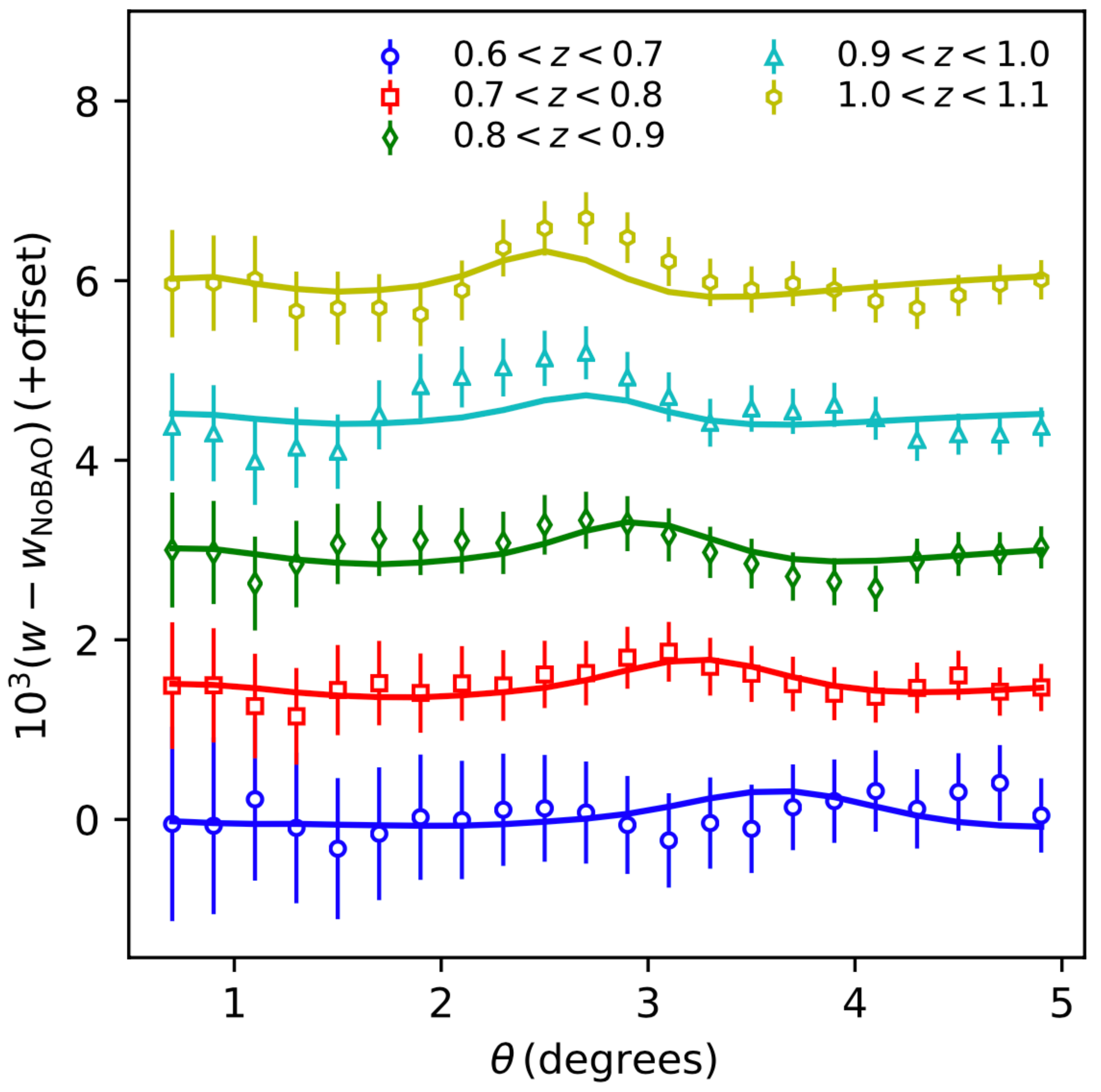

w

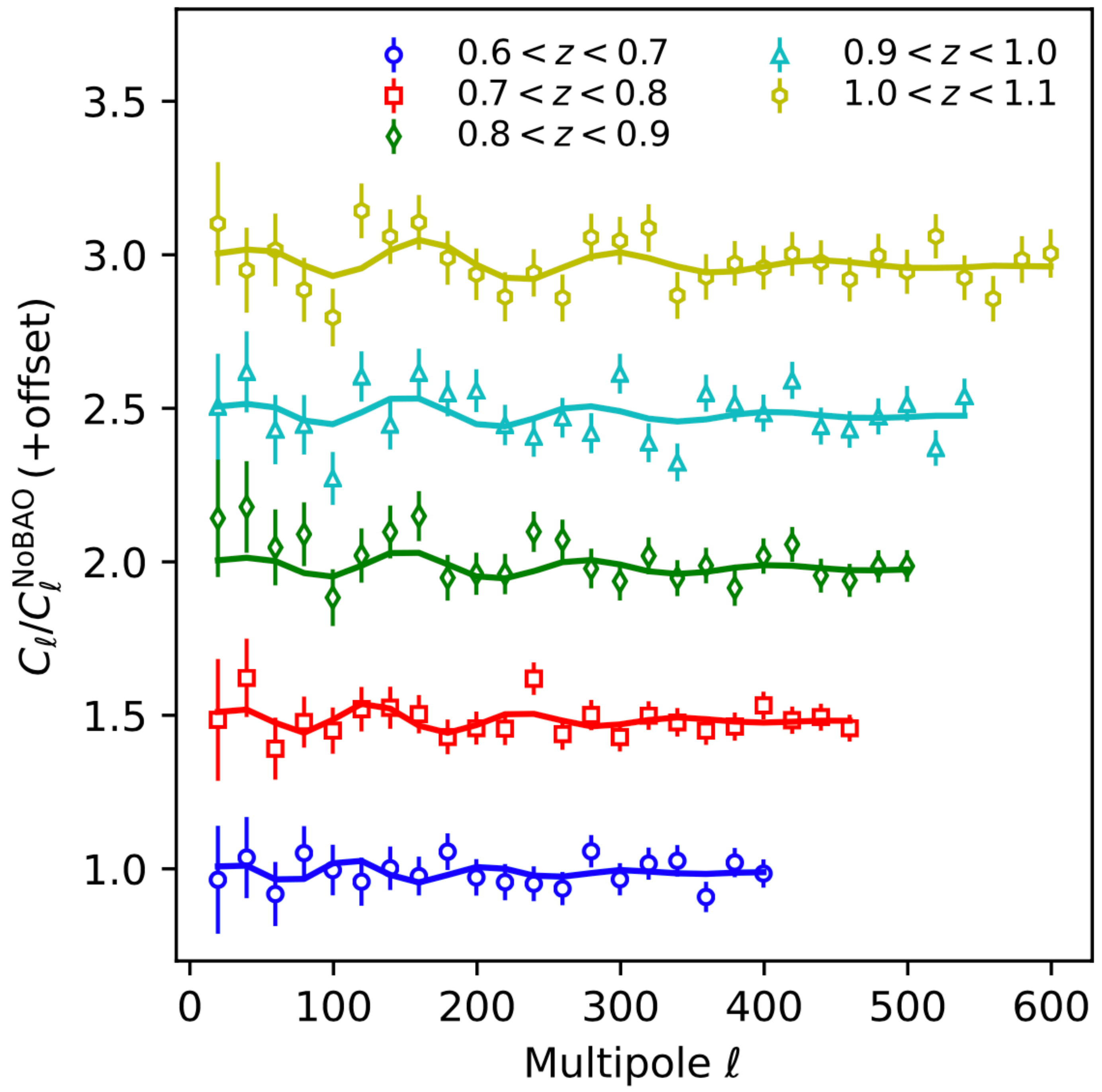

C_ℓ

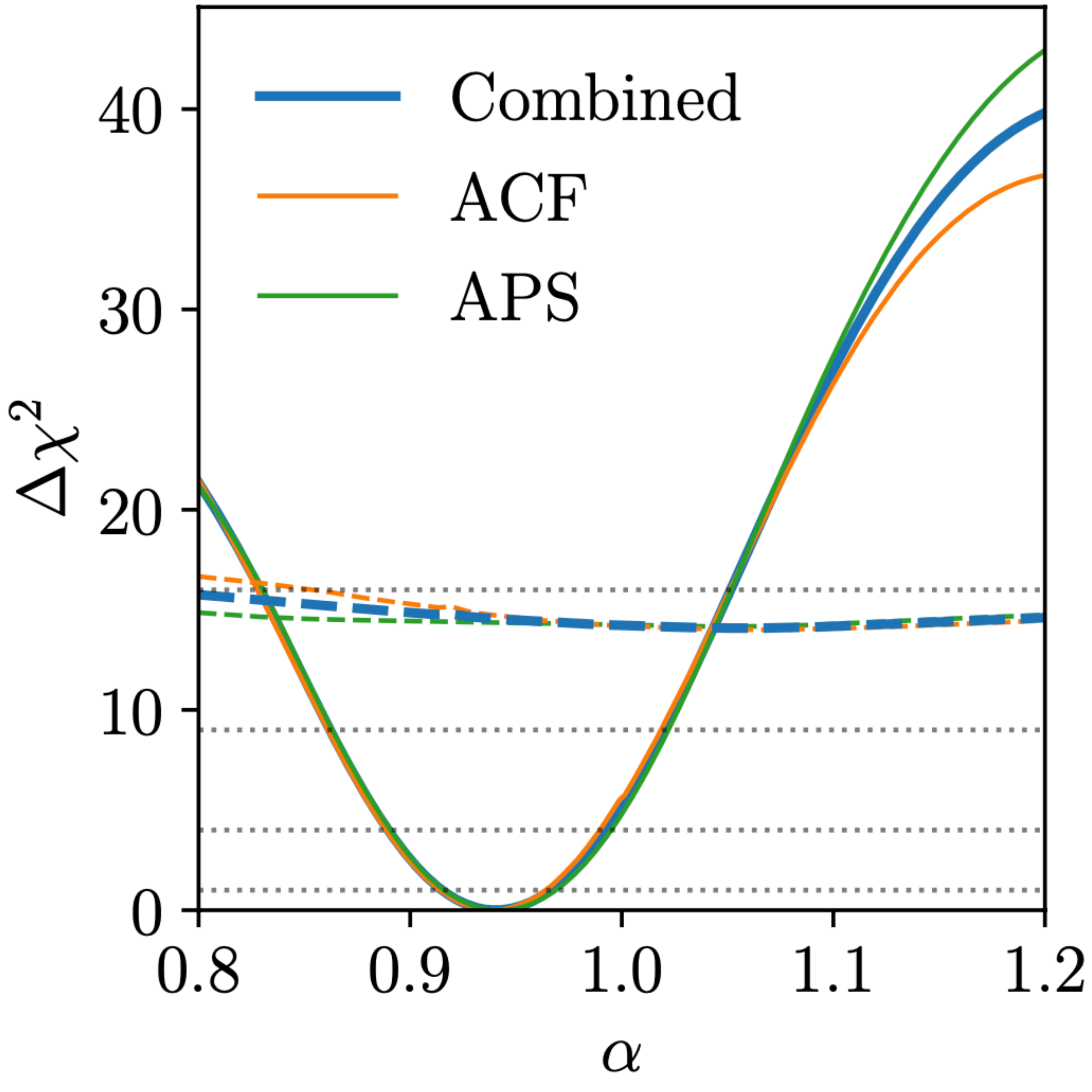

$$\alpha = \frac{\frac{D_{\rm M}}{r_{\rm d}}\big|_{\rm data}}{\frac{D_{\rm M}}{r_{\rm d}}\big|_{\rm fid}}$$

DES collaboration, 2107.05477

~ 2 sigma deviation from the Planck results

DES Y3 BAO constraints

- $D_\mathrm{M}/r_\mathrm{d} = 18.92 \pm 0.51$, 2.5% measurement of the BAO at z= 0.83
- Most precise BAO measurement from photometric surveys
- $D_\mathrm{M}/r_\mathrm{d}$ is at 2.3σ deviation from the Planck results, need more data and alternative analyses to corroborate

$$\alpha = \frac{\frac{D_\mathrm{M}}{r_\mathrm{d}}\Big|_\mathrm{data}}{\frac{D_\mathrm{M}}{r_\mathrm{d}}\Big|_\mathrm{fid}}$$

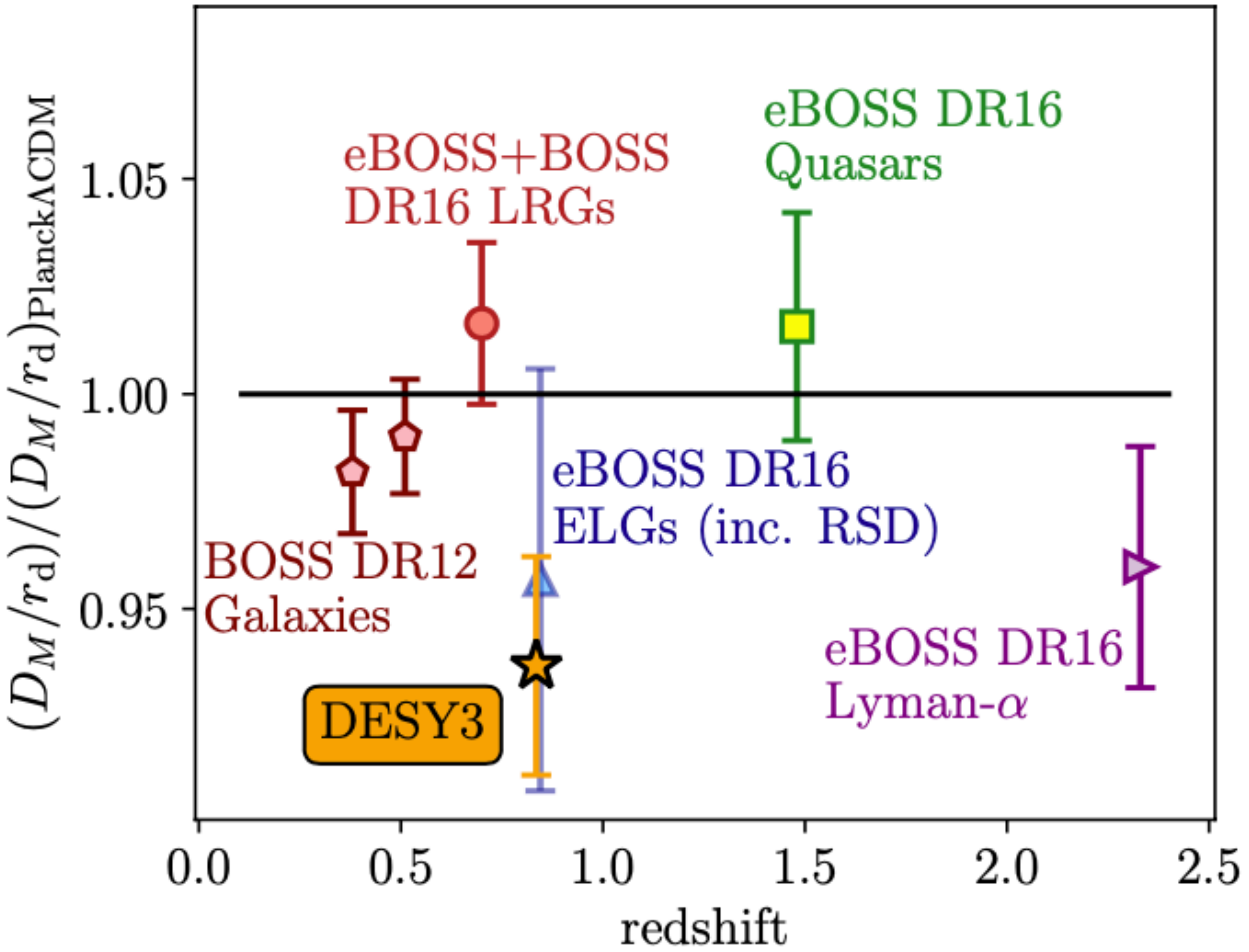

DES collaboration, 2107.05477

Projected three-dimensional clustering analysis

Three-dimensional correlation analysis

- Compute the 3D correlation function ξ akin to 3D analysis

Ross +, 1705.05442

- Compress info in the whole redshift range into a single data vector. Include some radial info

- Need to take care of the evolving dn/dz

- Radial direction is smeared, need projection

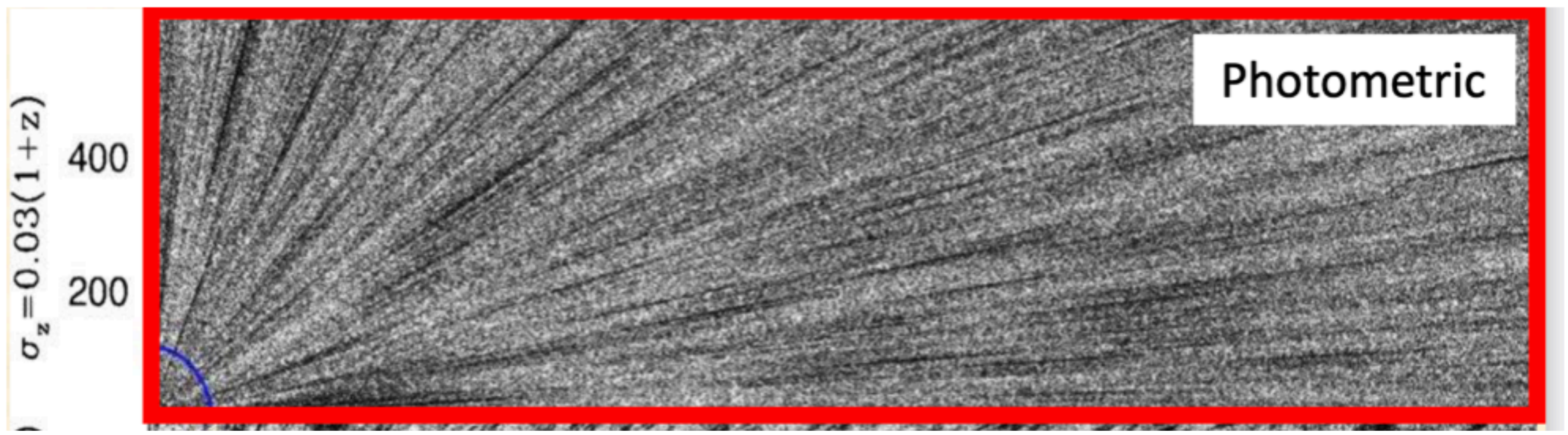

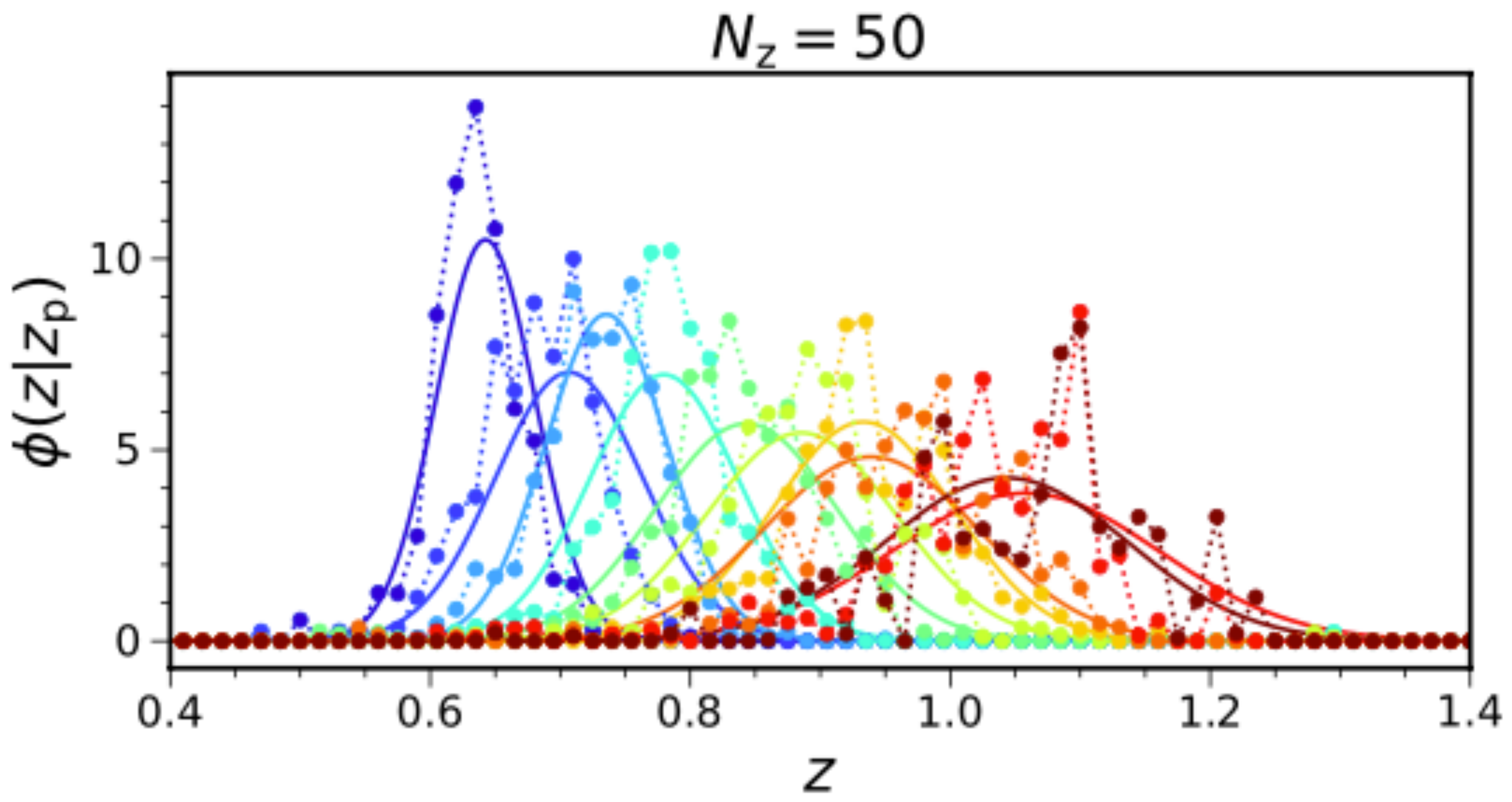

3D correlation analysis for photometric data

- For $\sigma_z \geq 0.02$, only effectively probes the transverse information, the transverse BAO is preserved

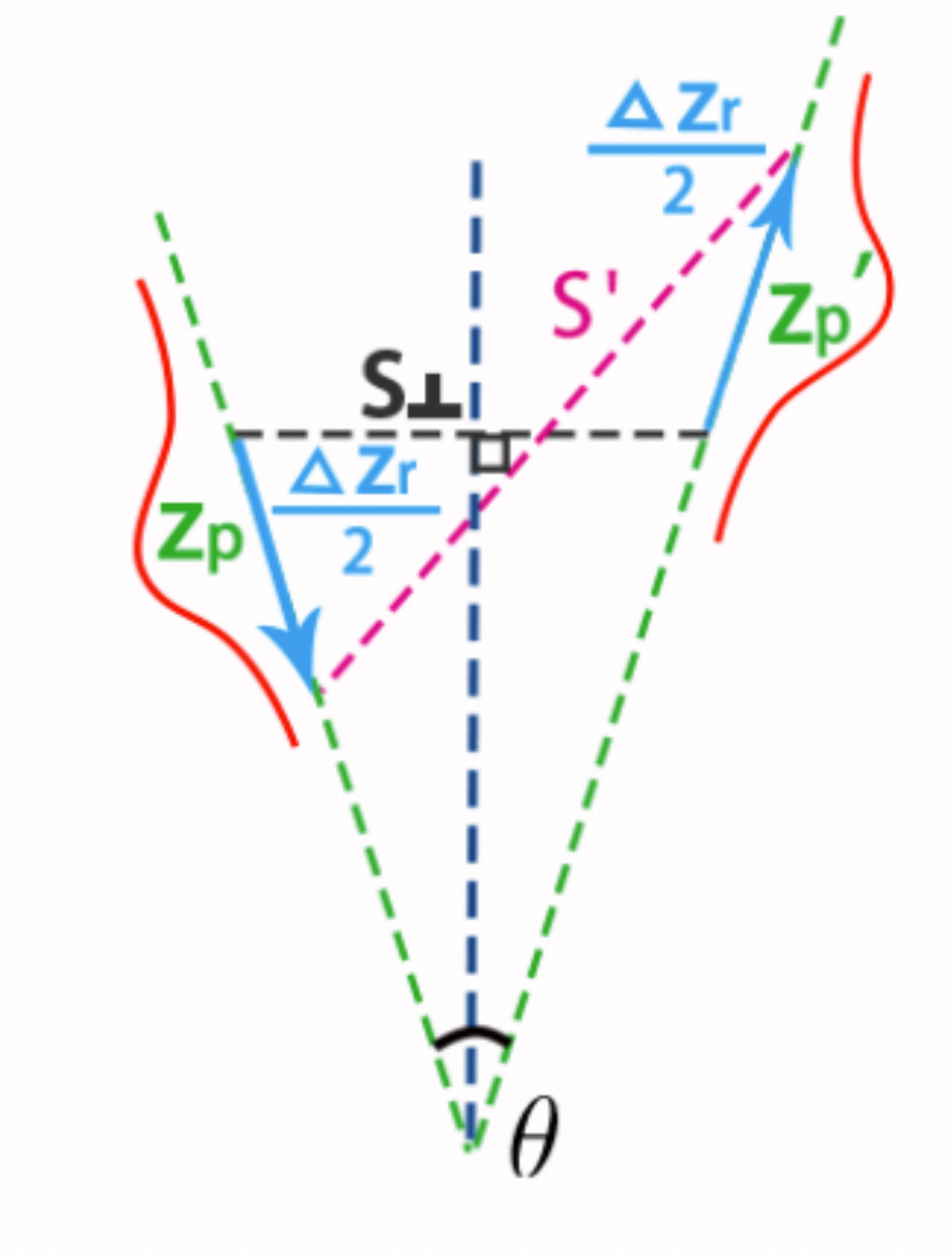

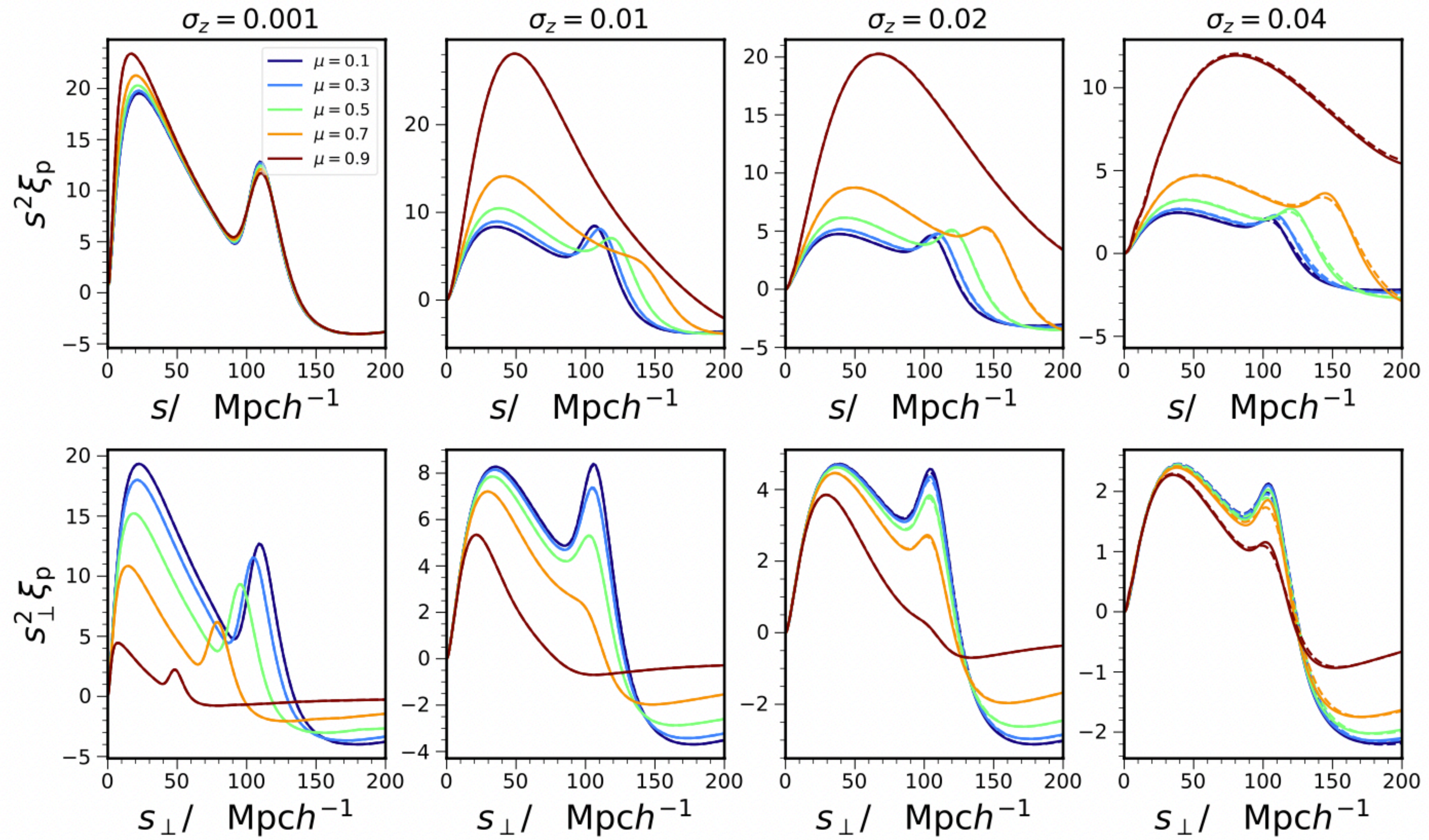

Ross +, 1705.05442 KCC +, 2110.13332

$\xi_{\rm p}$ template

- Obtained by mapping the general w template to $\xi_{\rm p}$

$$w_{ij}(\theta) = \sum_{\ell=0,2,4} i^\ell \int dz \phi(z|z_{\rm p}) \int dz' \phi(z'|z'_{\rm p}) \times \mathcal{L}_\ell(\hat{\mathbf{s}} \cdot \hat{\mathbf{e}}) \int \frac{dk k^2}{2\pi^2} j_\ell(ks) P_\ell(k, z, z'),$$

- Loop over ijk that satisfy the bin conditions, ensure the evolving dn/dz window is accounted for

$$\xi_{\rm p}(s, \mu) = \frac{\sum_{ijk} f_{ijk} w_{ij}(\theta_k)}{\sum_{ijk} f_{ijk}}$$

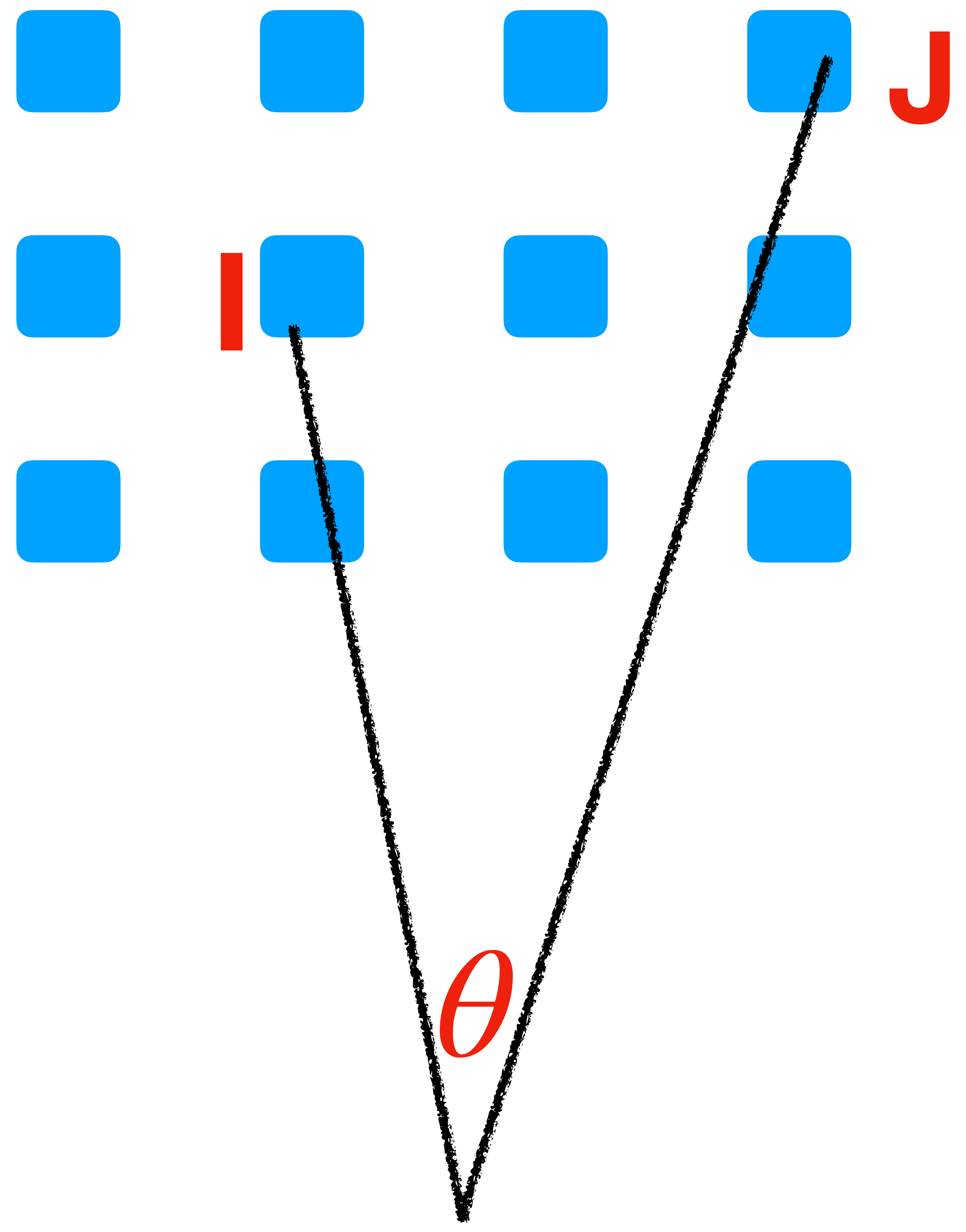

KCC +, 2110.13332

ξ_{p} template

- Photo-z uncertainties, the radial info, especially the radial BAO is erased

- Project $\xi_{\mathrm{p}}(s, \mu)$ to the transverse direction

KCC +, 2110.13332

$$\xi_{\mathrm{p}}(s_{\perp}) = \frac{\sum_i \xi_{\mathrm{p}}(s, \mu_i) W(\mu_i)}{\sum_i W(\mu_i)}$$

Tophat: equal weighting, sub-optimal

Gaussian: suppress the pairs with low signal to noise

Theory vs mock measurement

- ICE-COLA mocks, data include realistic photo-z uncertainties
- The theory template is in good agreement with the mock measurement

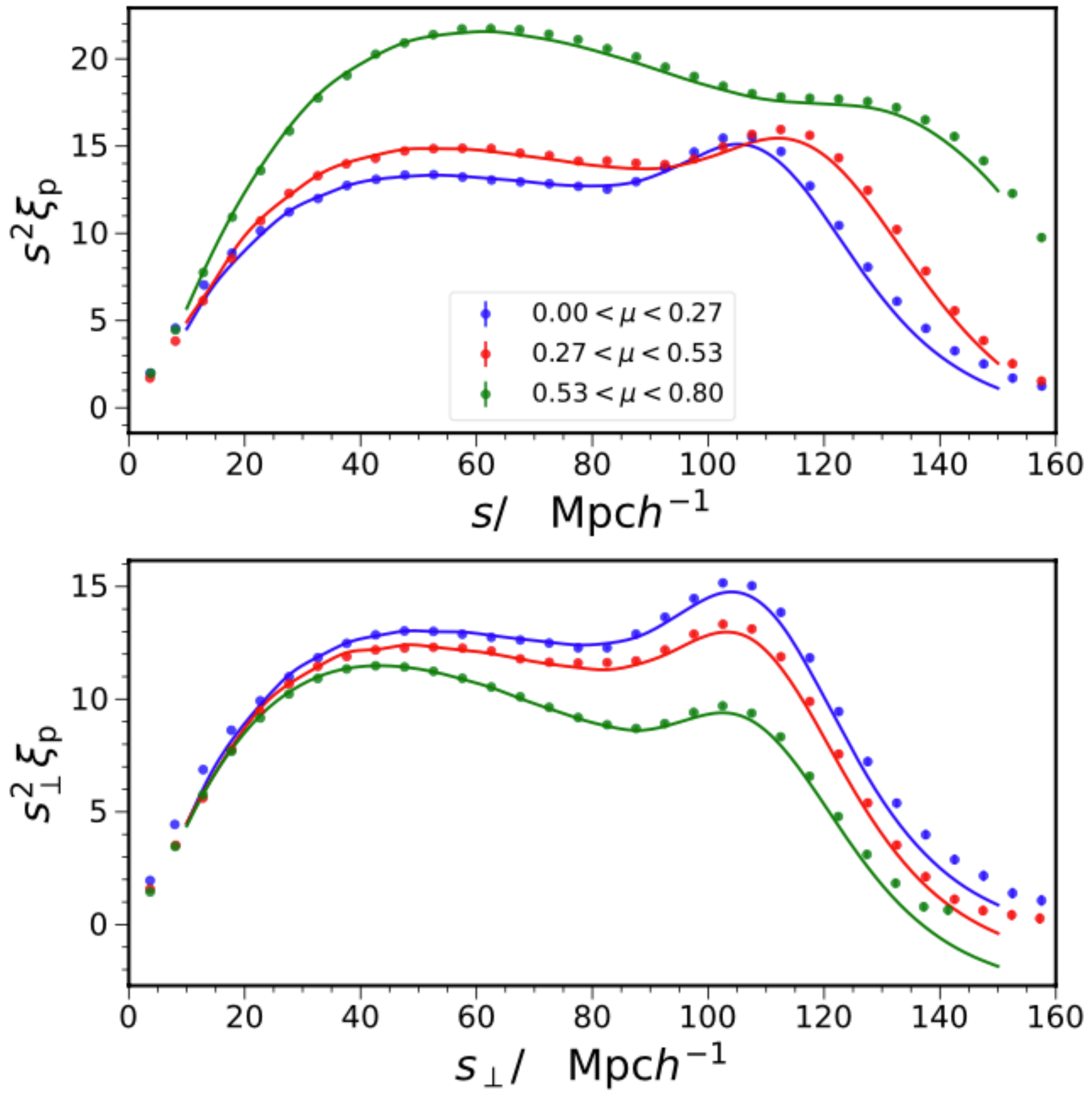

ξ_{p} covariance

- Mapping the general w covariance to ξ_{p} one

$$\mathrm{Cov}[\xi_{\mathrm{p}}(s_\perp), \xi_{\mathrm{p}}(s'_\perp)] = \frac{\sum_i \sum_j W(\mu_i) W(\mu_j) \mathrm{Cov}(\xi_{\mathrm{p}}(s, \mu_i), \xi_{\mathrm{p}}(s', \mu_j))}{\sum_i W(\mu_i) \sum_j W(\mu_j)}$$

$$\mathrm{Cov}[\hat{w}_{ij}(\theta), \hat{w}_{mn}(\theta')] = \sum_\ell \frac{(2\ell+1)}{(4\pi)^2 f_{\mathrm{sky}}} \bar{\mathcal{L}}_\ell(\cos\theta) \bar{\mathcal{L}}_\ell(\cos\theta') \left[\left(C_\ell^{im} + \frac{\delta_{\mathrm{K}}^{im}}{\bar{n}_i} \right) \left(C_\ell^{jn} + \frac{\delta_{\mathrm{K}}^{jn}}{\bar{n}_j} \right) + \left(C_\ell^{in} + \frac{\delta_{\mathrm{K}}^{in}}{\bar{n}_i} \right) \left(C_\ell^{jm} + \frac{\delta_{\mathrm{K}}^{jm}}{\bar{n}_j} \right) \right]$$

Finite bin width correction
Mask correction

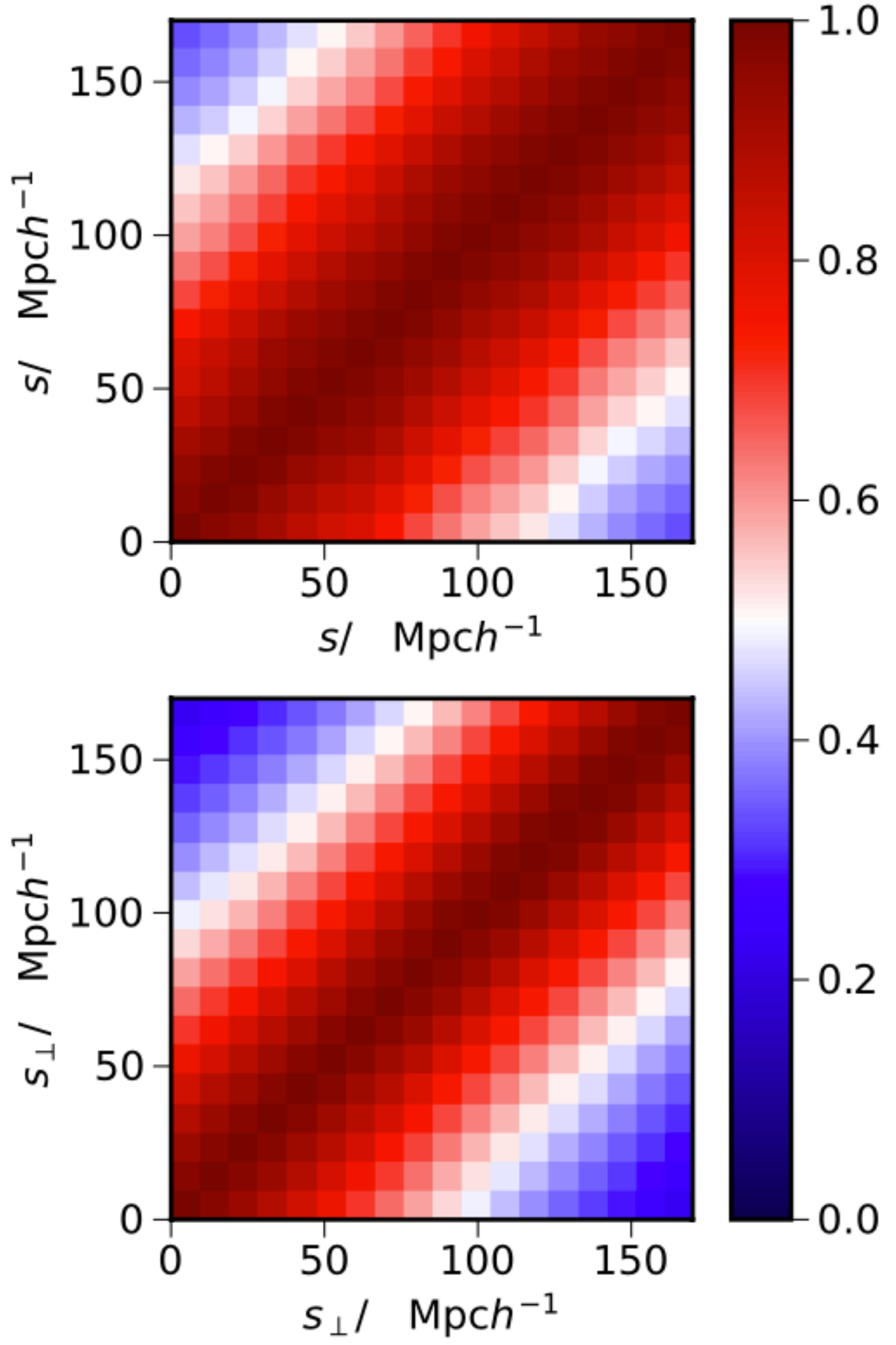

Correlation btw ξ_p and angular statistics

- The correlation btw ξ_p and angular statistics (w or C_ℓ) is low, serves as a relatively independent crosscheck on tomographic analyses

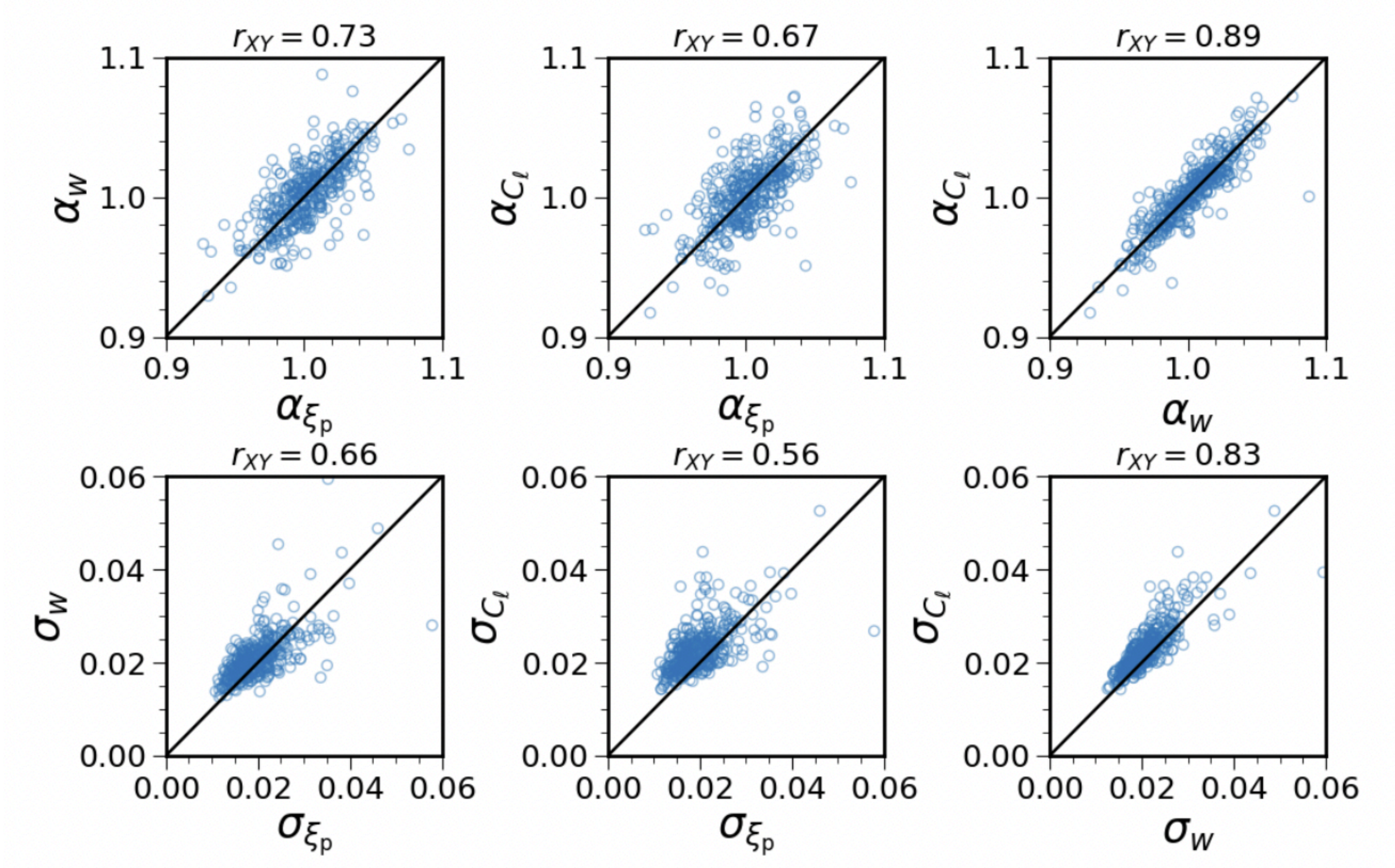

BAO sample

- BAO sample, 7.03 million red galaxies in the redshift range of [0.6,1.1] over a footprint of 4108 deg^2

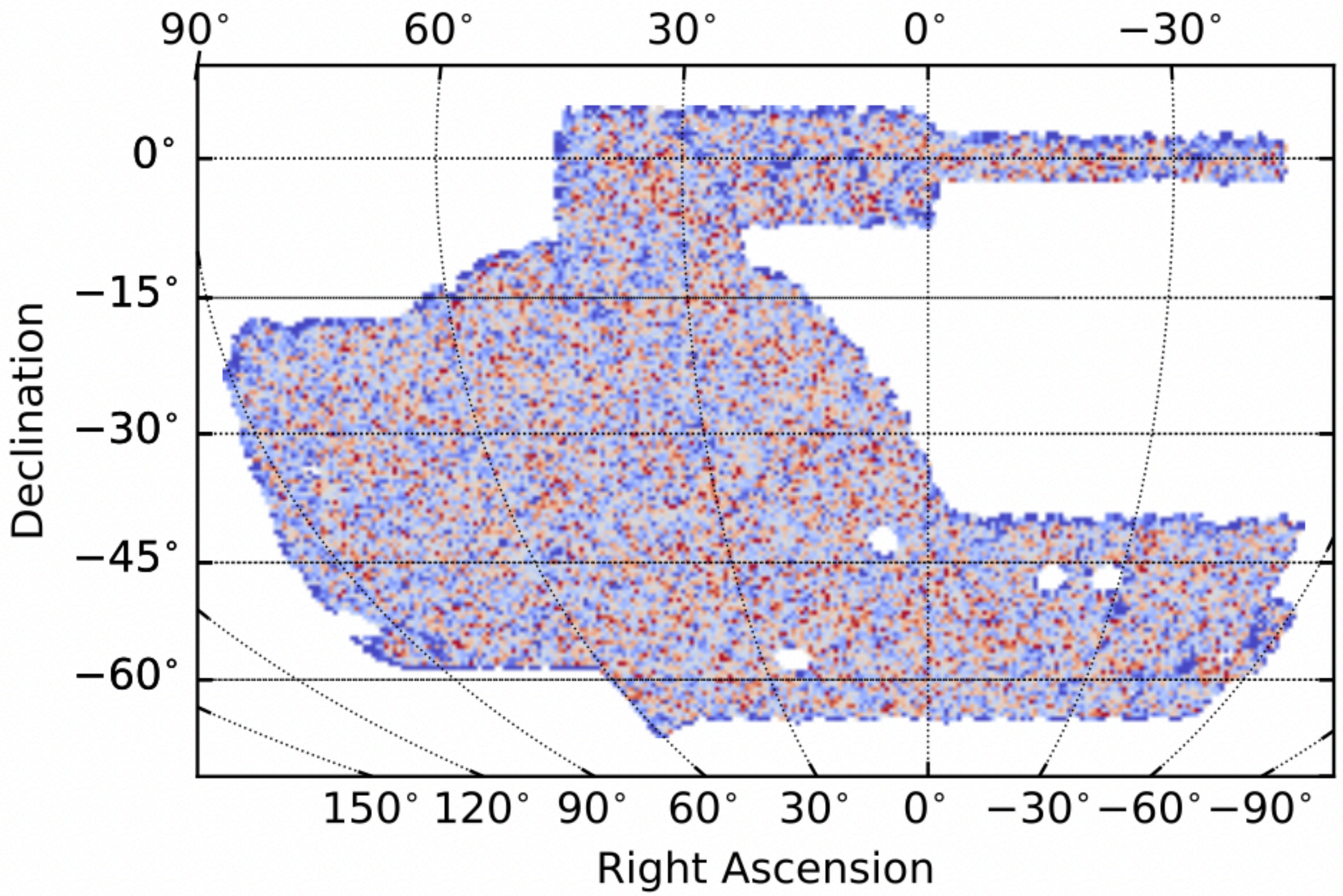

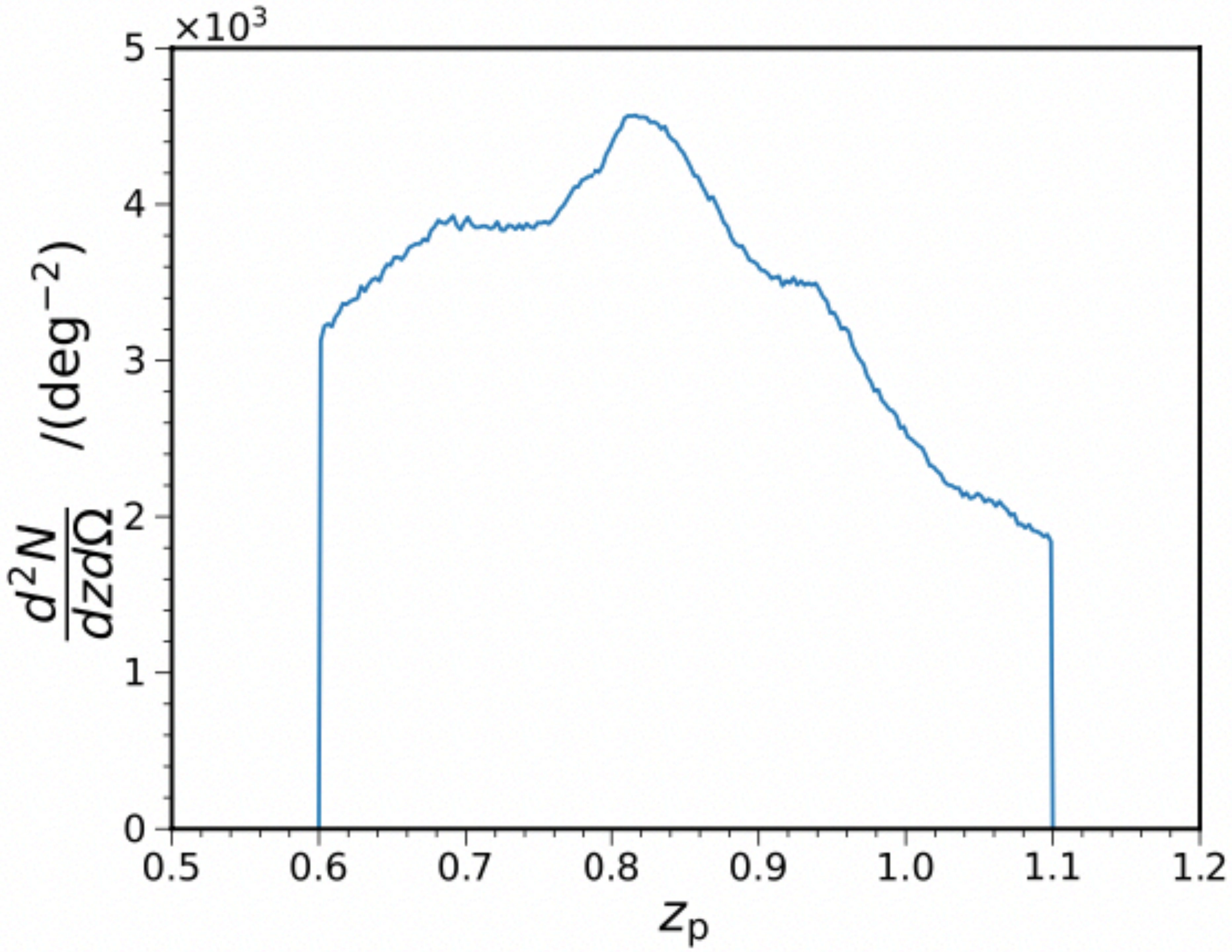

True-z distribution

- Photo-z derived from DNF, true redshift distribution estimated with the VIPERS spec-z sample

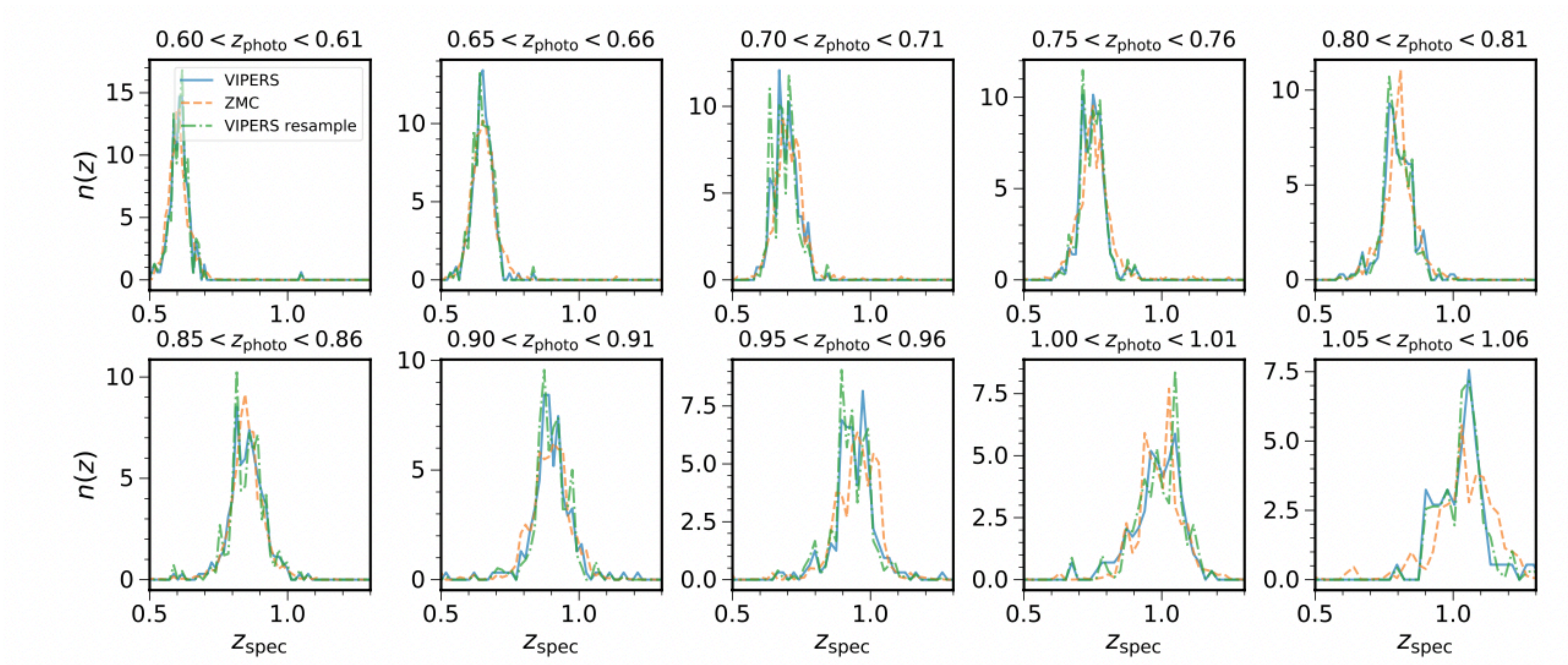

BAO measurements

- $\xi_{\rm p}$ constraint on α: 0.953 ± 0.029 (Gaussian) and 0.945 ± 0.033 (Top-hat)

- Consistent with w: 0.937 ± 0.025

- Deviation from Planck is reduced to 1.6 σ

Planck fiducial cosmology, $\alpha = 1$

$$\alpha = \frac{\frac{D_{\rm M}}{r_{\rm d}}\Big|_{\rm data}}{\frac{D_{\rm M}}{r_{\rm d}}\Big|_{\rm fid}}$$

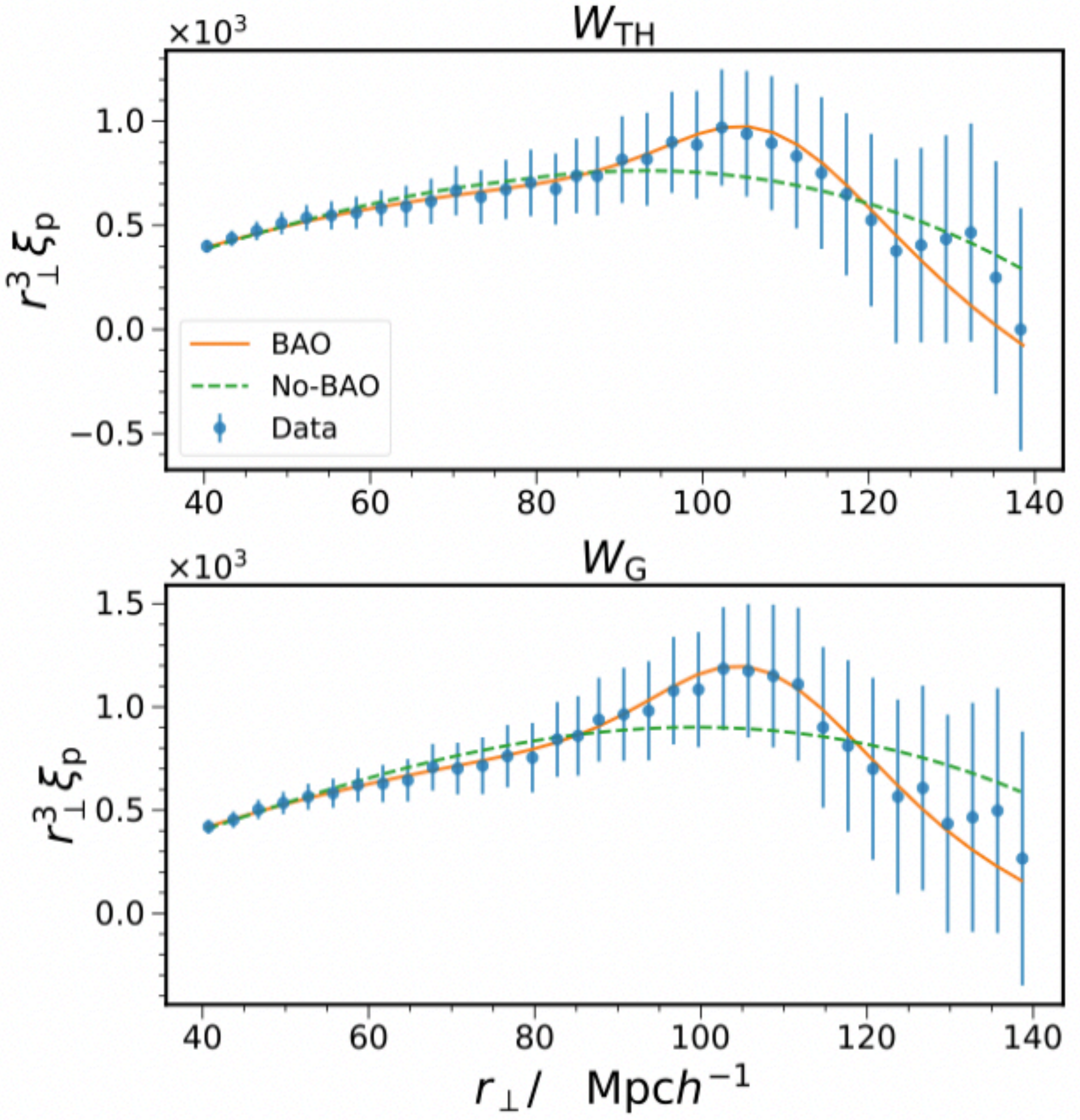

Individual bin fit results

- Individual tomographic bins, $\xi_{\rm p}$ gives comparable or even tighter constraint than w

- The BAO signals are heterogeneous across redshift, deviation from Planck mainly driven by the last bin

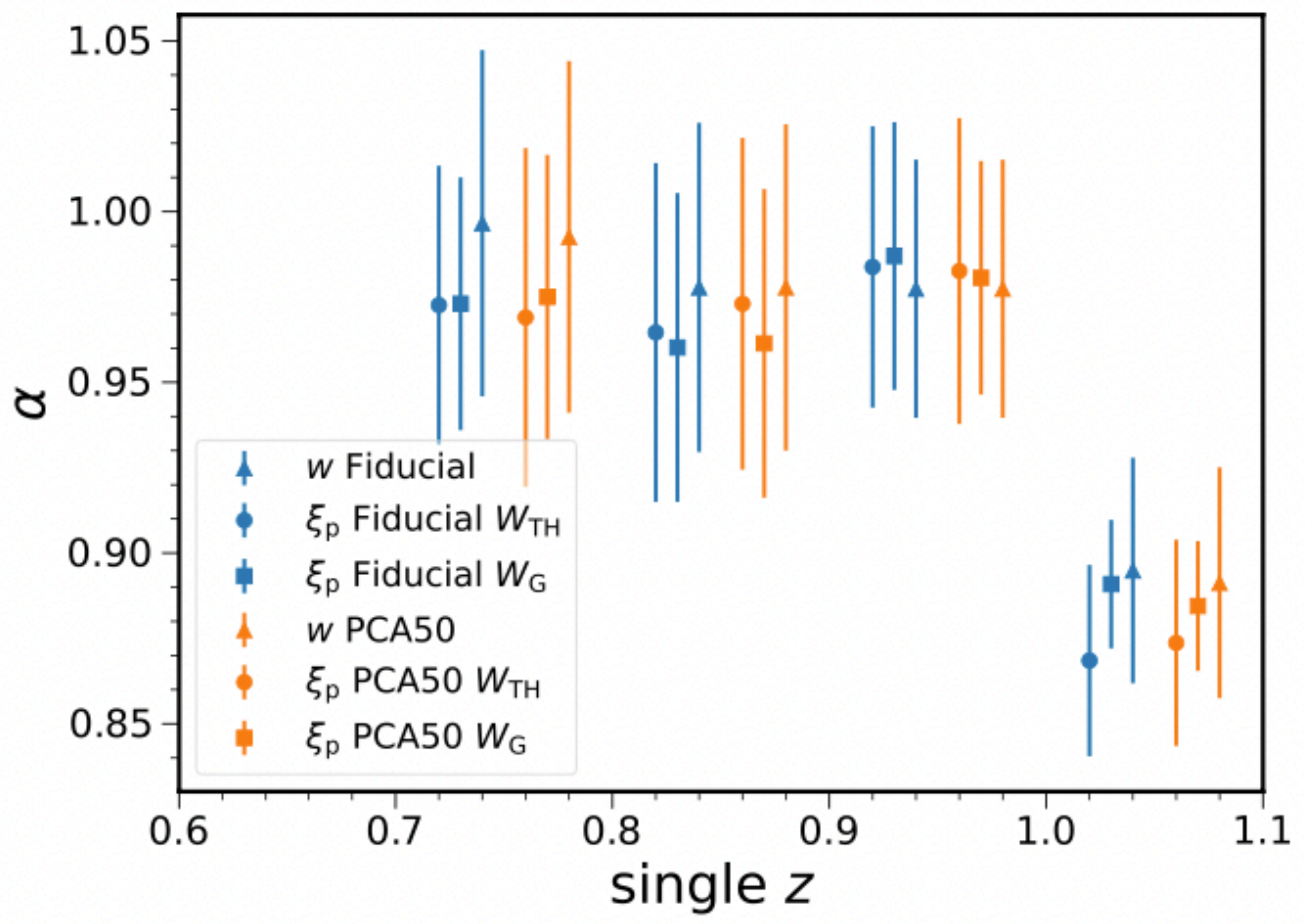

Error bars in heterogeneous mocks

- In heterogeneous mocks, the probability of getting ξ_p with error bar larger than w is enhanced

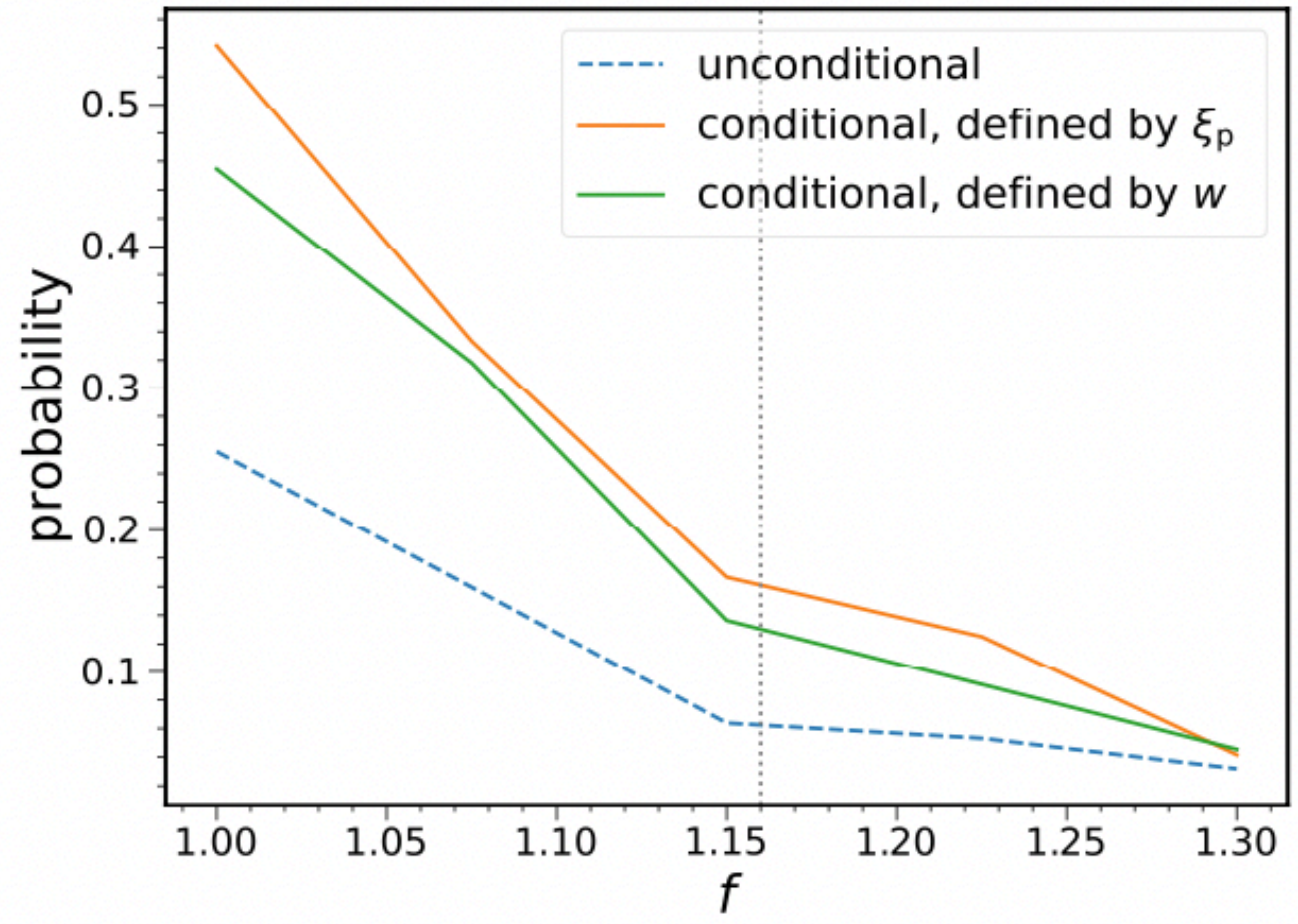

Measurements in homogeneous sample

- The combo 2-4 bins contains more constant BAO signals, the resultant constraint from 0.977 ± 0.026 (Gaussian) and 0.975 ± 0.033 (Top-hat) vs 0.978 ± 0.027 (w)
- ξ_{p} combines the signals at the level of data vector, while w effectively combines likelihood
- Caveat: combining likelihood always shrinks the error bar

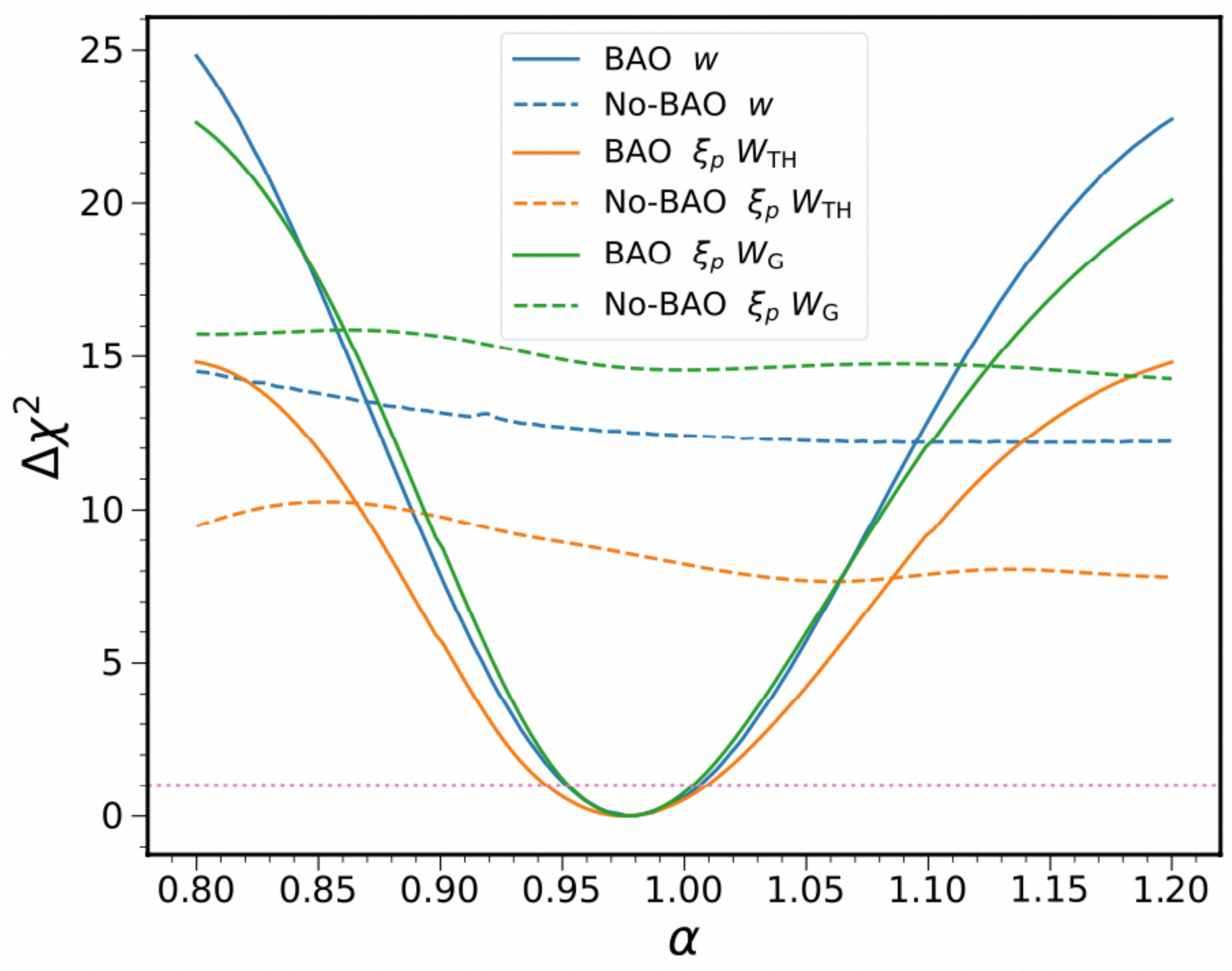

Robustness tests

- $\xi_{\rm p}$ is generally more sensitive to photo-z noise than w b/c (1) it measures correlation after projection (2) it combines signals at the level of data vector

- Gaussian window is more stable than top-hat as it puts more weight to the transverse pairs

Case	$\xi_{\rm p}$: $W_{\rm G}$	$\xi_{\rm p}$: $W_{\rm TH}$	w
Default	0.953 ± 0.029 (21.5/29)	0.945 ± 0.033 (33.4/29)	0.937 ± 0.025 (95.2/89)
No sys. corr.	0.942 ± 0.029 (39.7/29)	* 0.938 ± 0.033 (46.4/29)	0.935 ± 0.026 (94.6/89)
sys − PCA50	0.945 ± 0.029 (22.8/29)	0.943 ± 0.028 (36.0/29)	0.937 ± 0.025 (94.9/89)
$n(z)$ `Z_MC`	0.948 ± 0.029 (21.6/29)	* 0.943 ± 0.034 (33.6/29)	0.935 ± 0.025 (95.6/89)
MICE template	0.989 ± 0.038 (53.5/29)	* 0.988 ± 0.032 (78.5/29)	0.980 ± 0.026 (95.1/89)
MICE cov.	0.956 ± 0.021 (23.7/29)	* 0.955 ± 0.025 (41.0/29)	0.936 ± 0.021 (125.8/89)
MICE cosmology	0.996 ± 0.026 (59.3/29)	0.995 ± 0.021 (90.7/29)	0.977 ± 0.022 (125.8/89)
Unmodified cov.	0.956 ± 0.030 (21.3/29)	0.953 ± 0.035 (32.7/29)	—
$[70, 130]\,{\rm Mpc}\,h^{-1}$	0.955 ± 0.030 (11.7/16)	0.965 ± 0.031 (17.1/16)	—
$\Delta r = 5\,{\rm Mpc}\,h^{-1}$	0.953 ± 0.030 (19.1/15)	0.953 ± 0.036 (16.2/15)	—
$\Delta r = 2\,{\rm Mpc}\,h^{-1}$	0.949 ± 0.028 (38.1/44)	0.941 ± 0.031 (44.5/45)	—
No bin 1	0.976 ± 0.024 (29.5/29)	* 0.960 ± 0.030 (38.7/29)	0.948 ± 0.026 (67.8/71)
No bin 2	0.928 ± 0.034 (19.0/29)	* 0.931 ± 0.034 (32.4/29)	0.929 ± 0.026 (80.7/71)
No bin 3	0.938 ± 0.034 (27.0/29)	* 0.941 ± 0.038 (38.7/29)	0.935 ± 0.028 (78.4/71)
No bin 4	0.928 ± 0.033 (24.7/29)	* 0.943 ± 0.034 (38.8/29)	0.925 ± 0.028 (70.0/71)
No bin 5	0.950 ± 0.030 (21.5/29)	* 0.959 ± 0.029 (40.6/29)	0.967 ± 0.026 (82.3/71)

Angular vs Projected 3D

	Angular analysis Projection and then clustering measurement	Projected 3D Clustering measurement and then projection
Pros	**Angle only, cosmology-independent**	**Effective to condense the data Include some radial info**
Cons	**Explicit bin division, loss of radial info**	**Need cosmology for distance computation More sensitive to noise**

Both statistics offer important crosschecks on each other.

Y6 BAO analysis

- Same footprint, but deeper magnitude
- ξ_{p}, along with angular statistics, is adopted for fiducial Y6 BAO analysis

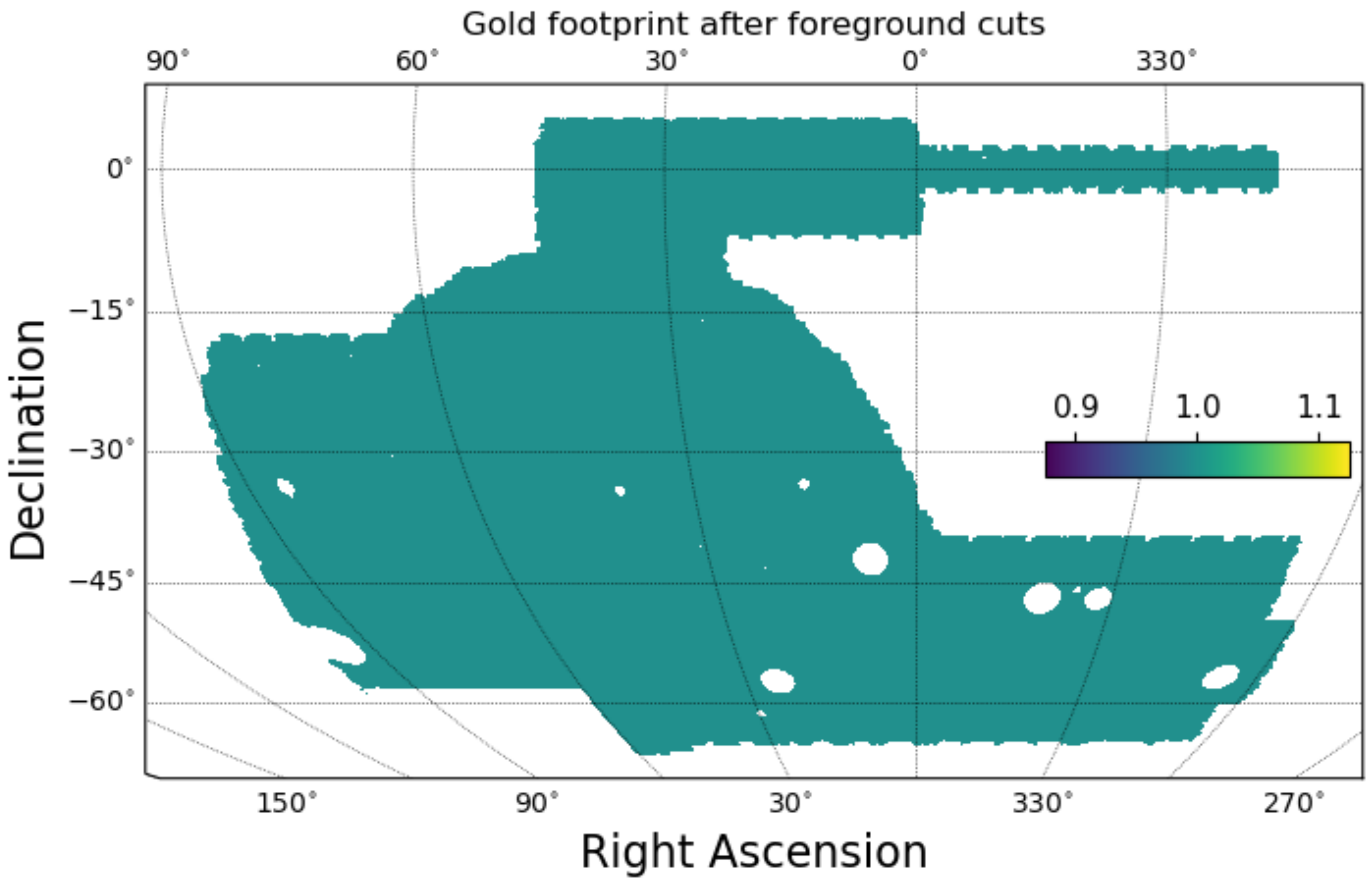

Photometric BAO reconstruction

KCC + , in preparation

Damping of the BAO

- Large scale bulk flow causes the BAO feature to be damped over time

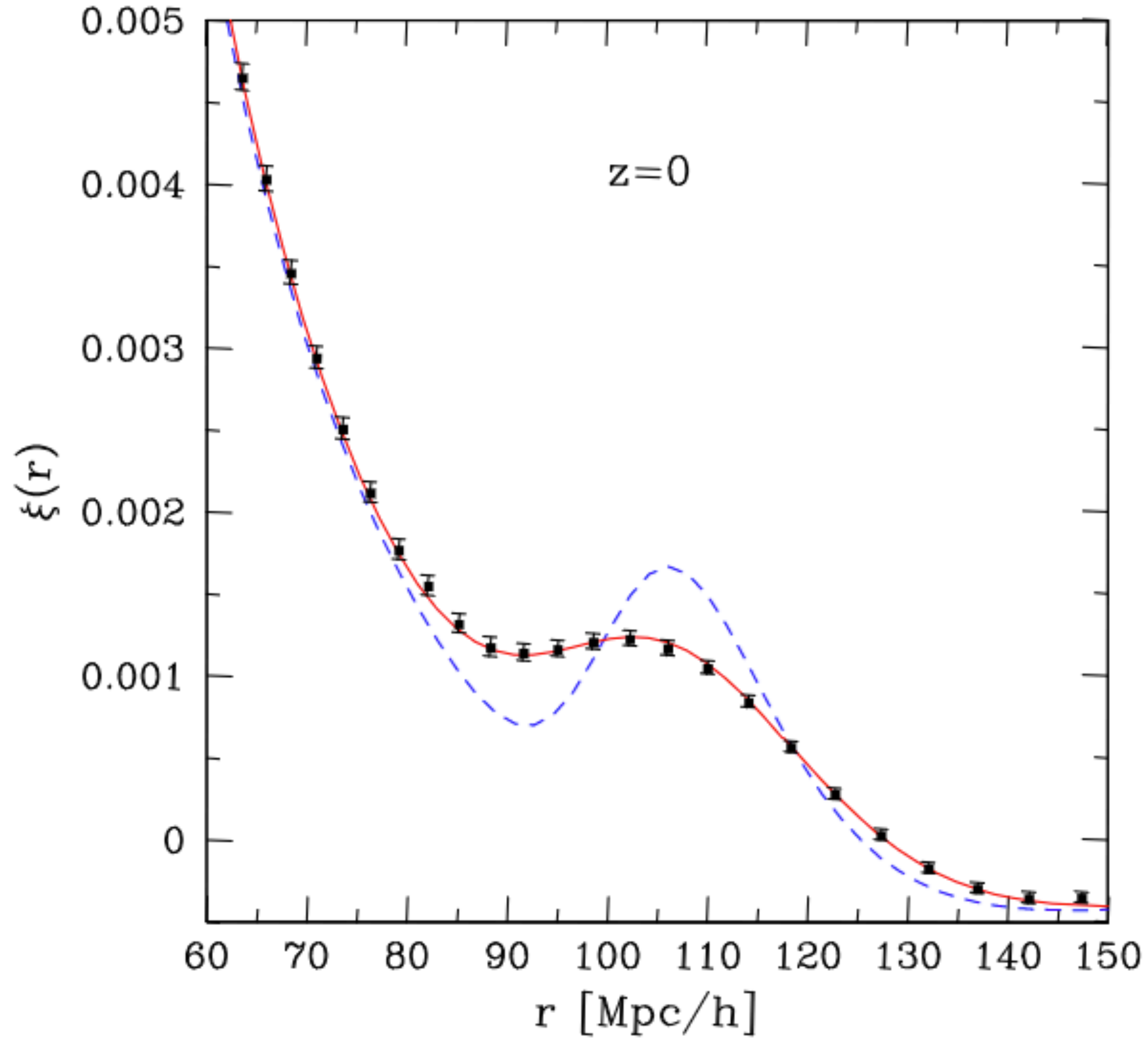

Crocce & Scoccimarro 2007

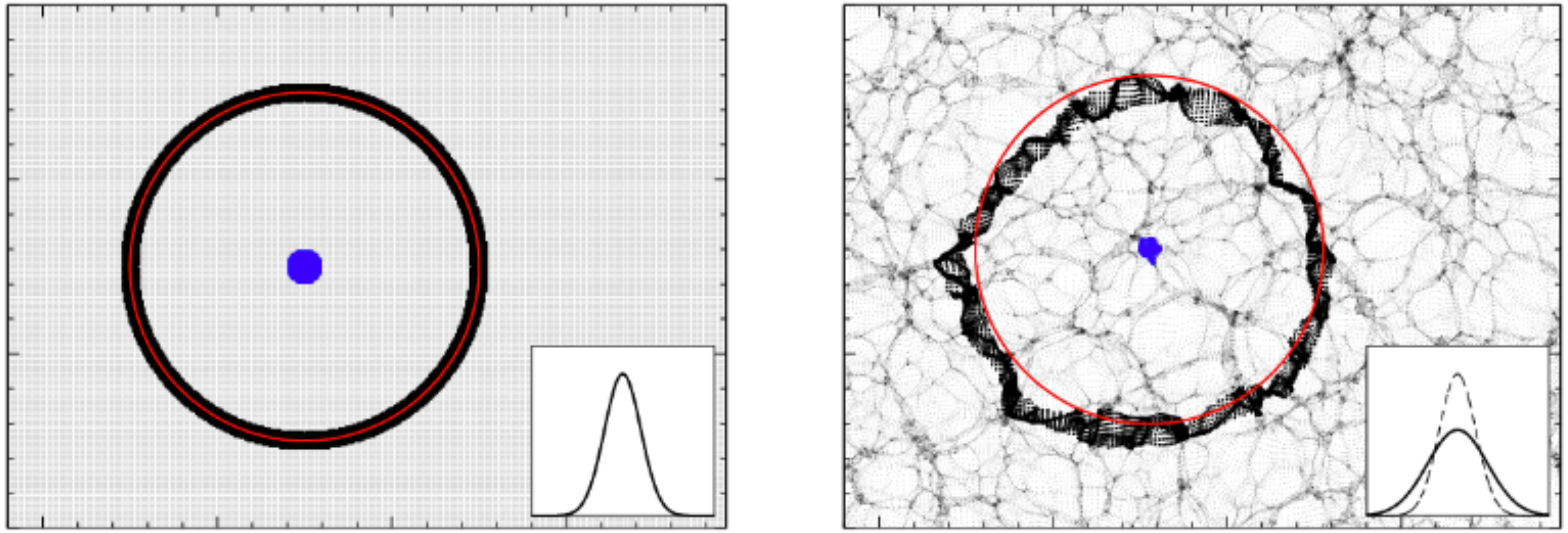

Padmanabhan +, 2012

BAO reconstruction

- To enhance the BAO significance, the BAO reconstruction method was proposed by Eisenstein + 2007

- Partially remove the LSS nonlinear evolution and put the particles back to the initial position

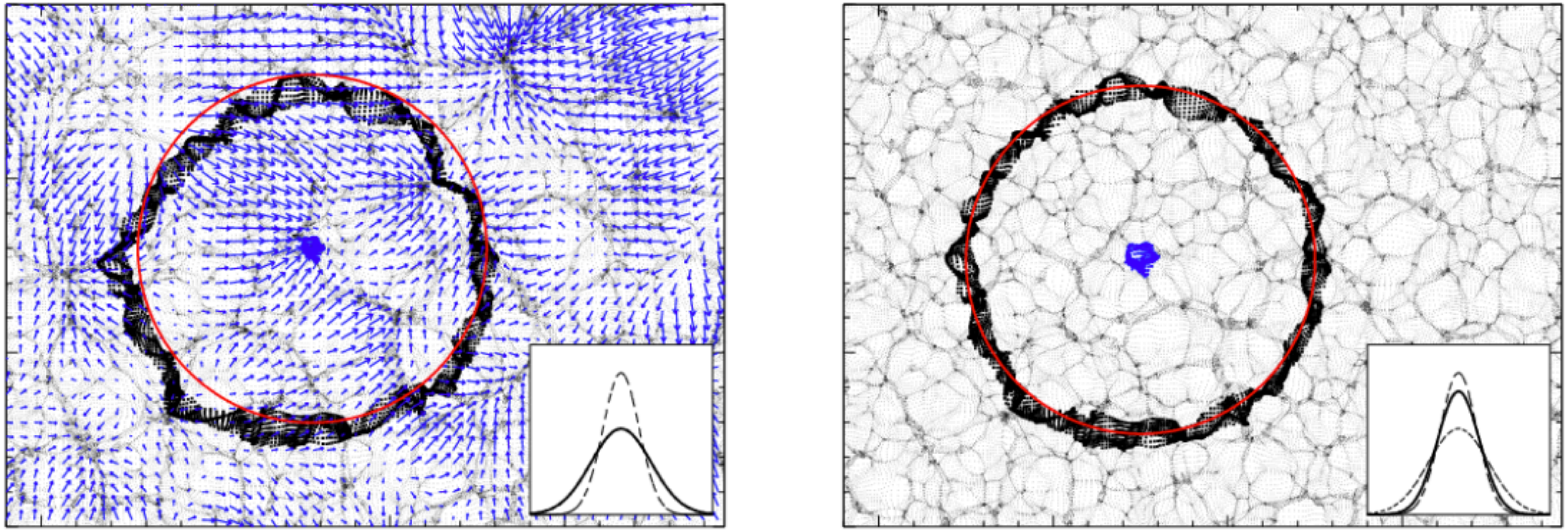

Padmanabhan +, 2012

The BAO reconstruction

- has been routinely applied to spectroscopic BAO analyses, notably SDSS, BOSS, eBOSS

Padmanabhan +, 2012

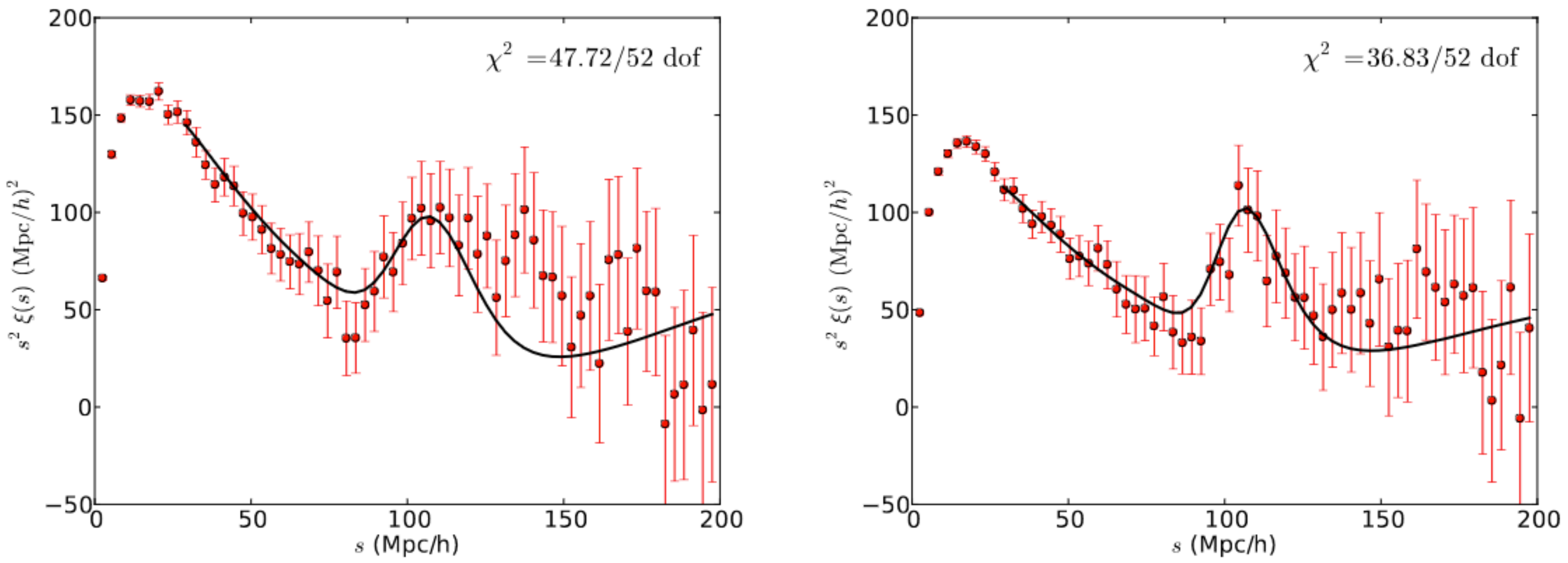

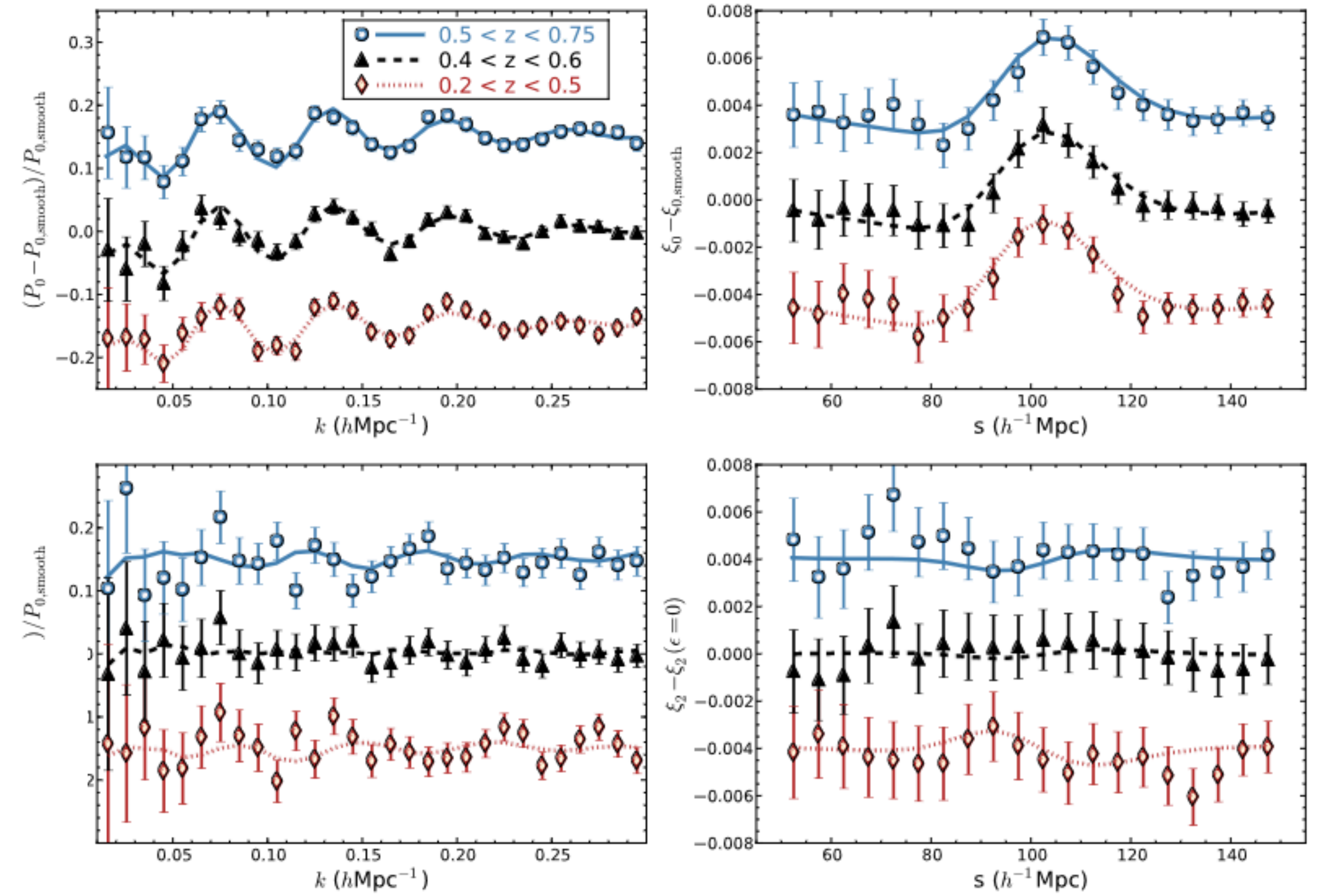

Alam +, BOSS, 2016

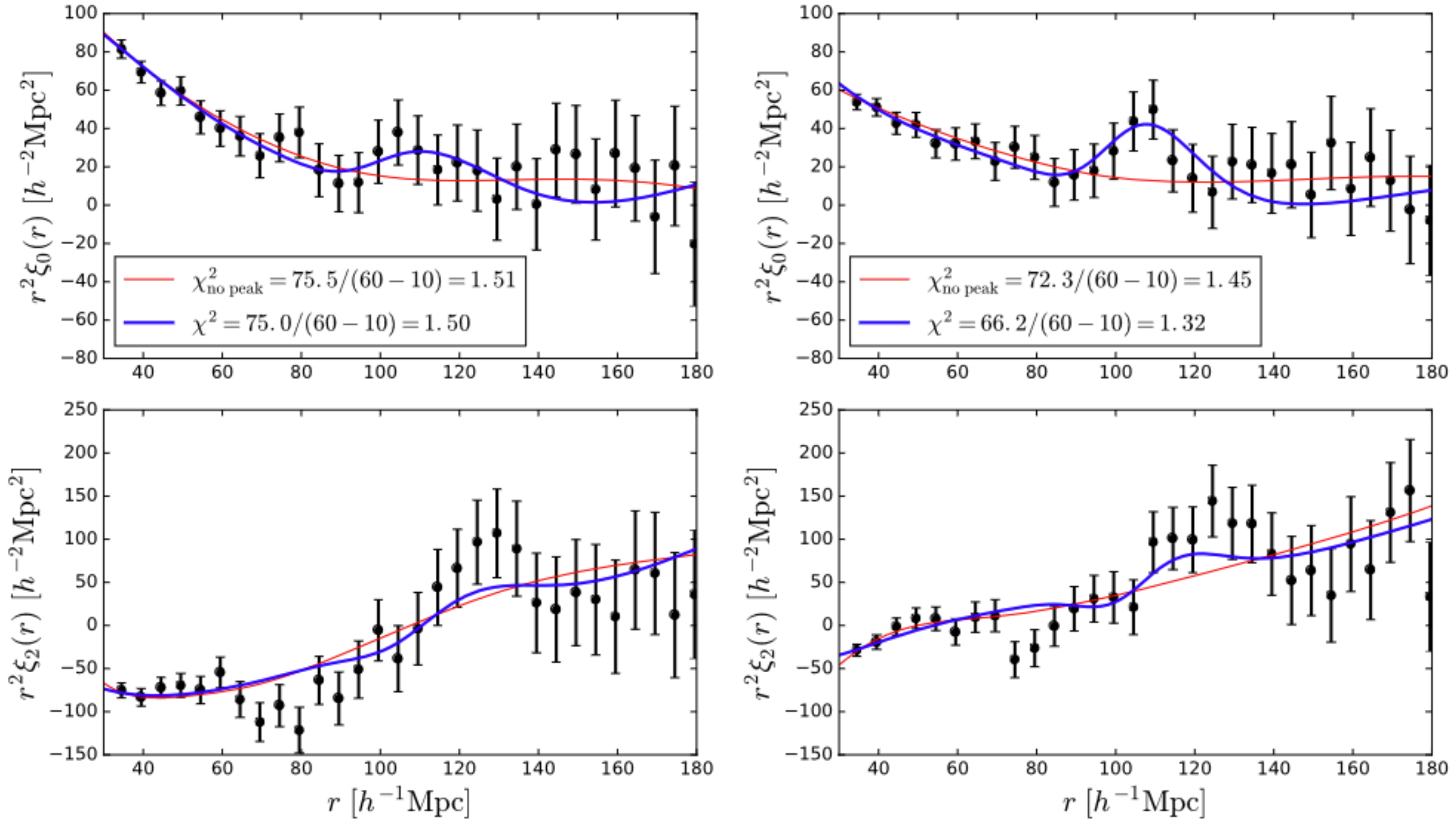

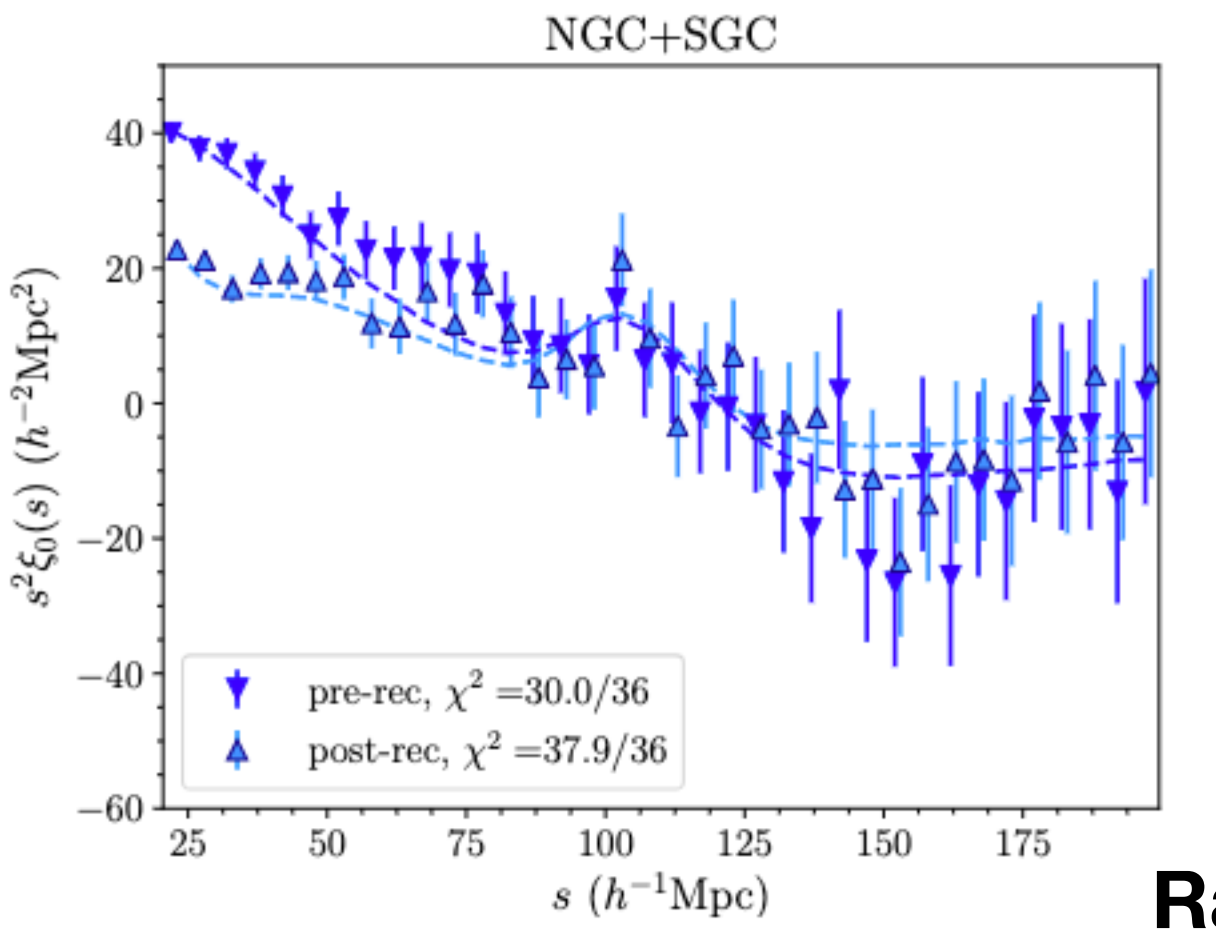

Bautista +, 2018

Raichoor +, eBOSS ELG, 2020

Transverse BAO reconstruction

- Standard BAO reconstruction requires potential derived from 3D density, is limited to spec-z sample studies so far
- Can be applied to photometric samples?
- Naive inversion of the 3D potential may mix the radial and transverse info
- Splitting the field into transverse and radial directions, the transverse displacement potential can be derived

$$\nabla_{\perp}^{2}\bar{\phi}_{2}(\boldsymbol{x}_{\perp}) = \bar{\delta}_{2}(\boldsymbol{x}_{\perp}) - \frac{1}{L}\frac{\partial}{\partial x_{\parallel}^{\mathrm{p}}}\phi_{2}(\boldsymbol{x}_{\perp}, x_{\parallel}^{\mathrm{p}})\Big|_{x_{\parallel,0}^{\mathrm{p}}}^{x_{\parallel,1}^{\mathrm{p}}}$$

Additional source due to gravity is nonlocal

Test on N-body data

- Consider comoving N-body simulation, Gaussian photo-z uncertainty in z-direction

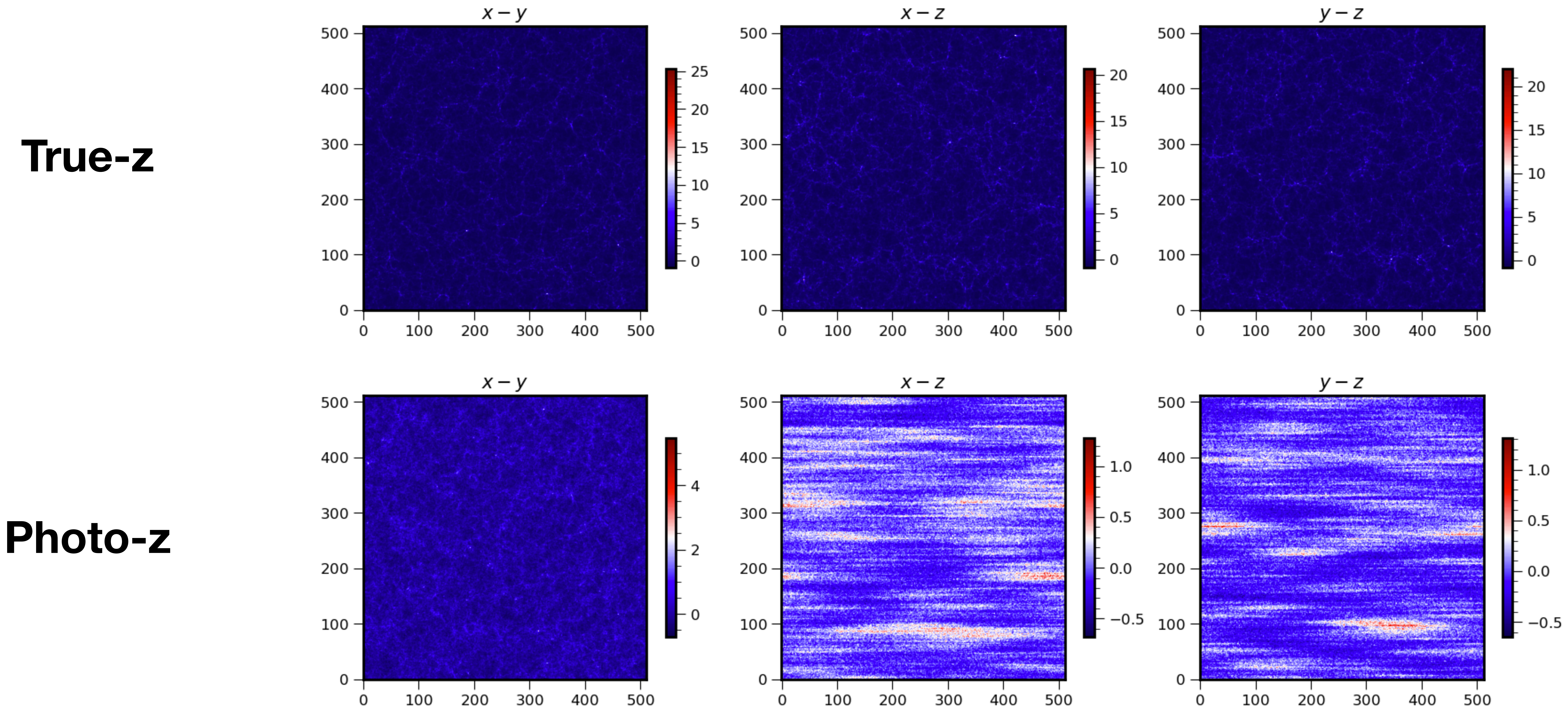

Sources of the transverse potential

- The source contribution is dominated by the density on the slab

$$\nabla_\perp^2 \bar{\phi}_2(\boldsymbol{x}_\perp) = \bar{\delta}_2(\boldsymbol{x}_\perp) - \frac{1}{L}\frac{\partial}{\partial x^{\rm p}_{||}}\phi_2(\boldsymbol{x}_\perp, x^{\rm p}_{||})\Big|^{x^{\rm p}_{||,1}}_{x^{\rm p}_{||,0}}$$

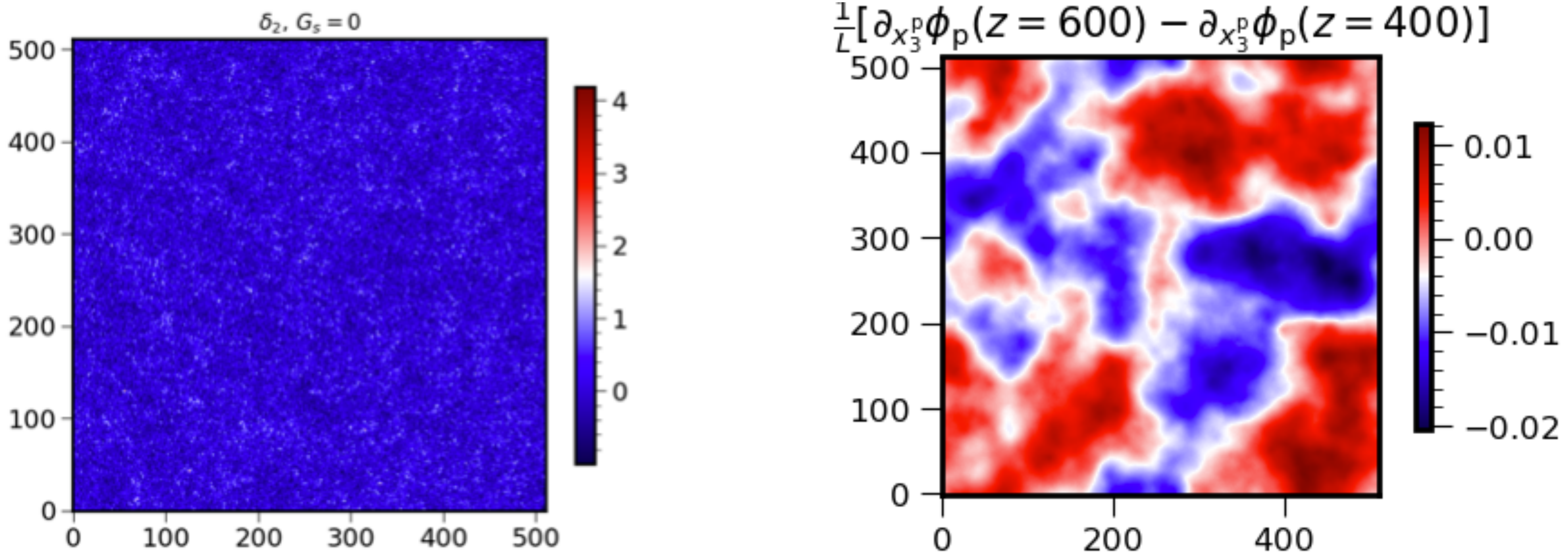

Reconstructed P(k)

- The reconstructed power spectrum enhances the BAO feature

Matter z=0

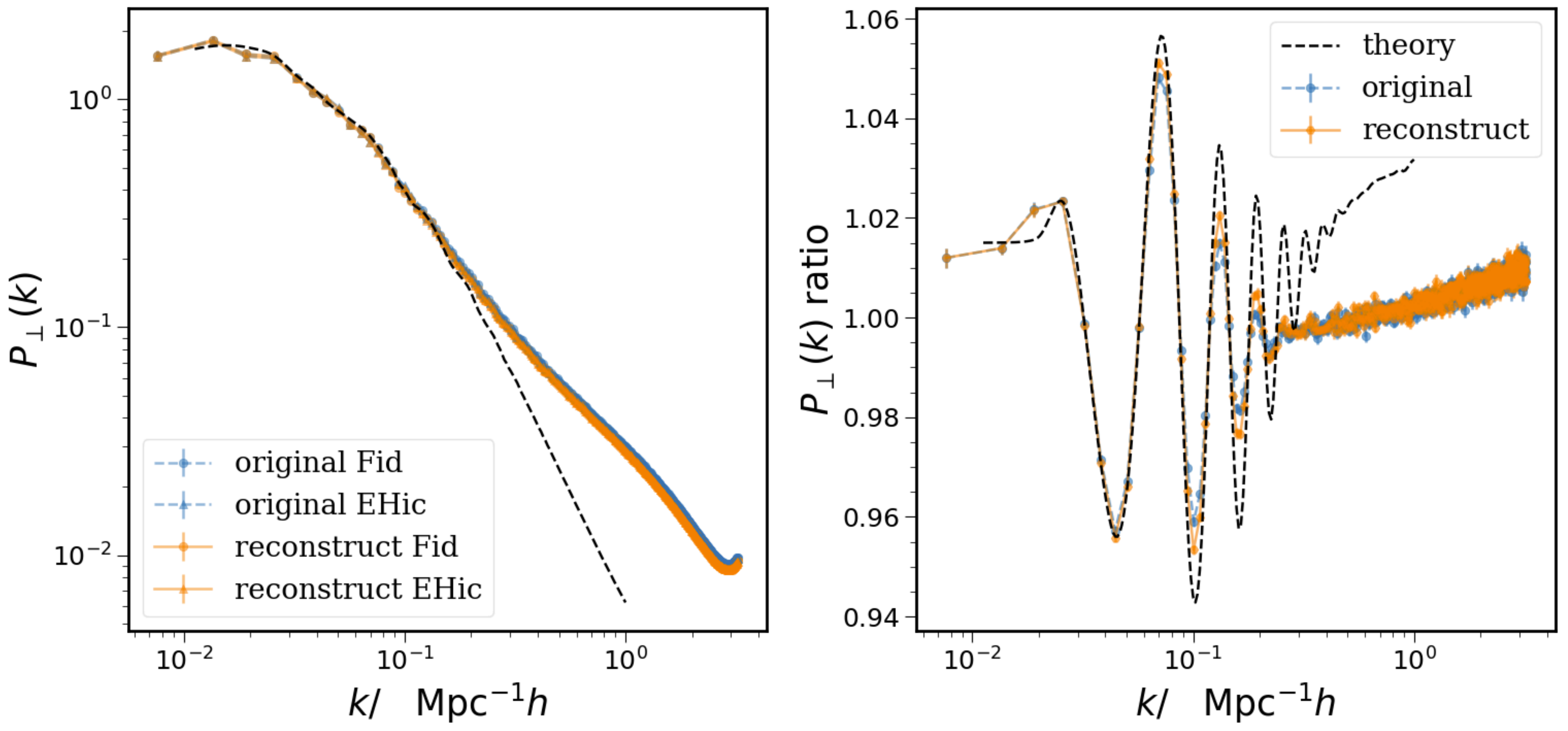

Reconstructed P(k)

- Although the halo results are much noisier, increase in BAO feature is still visible

Halo z=0, mean halo mass $5 \times 10^{13} M_{\odot} h^{-1}, \quad n_{\rm den} = 4 \times 10^{-4} ({\rm Mpc}h^{-1})^{-3}$

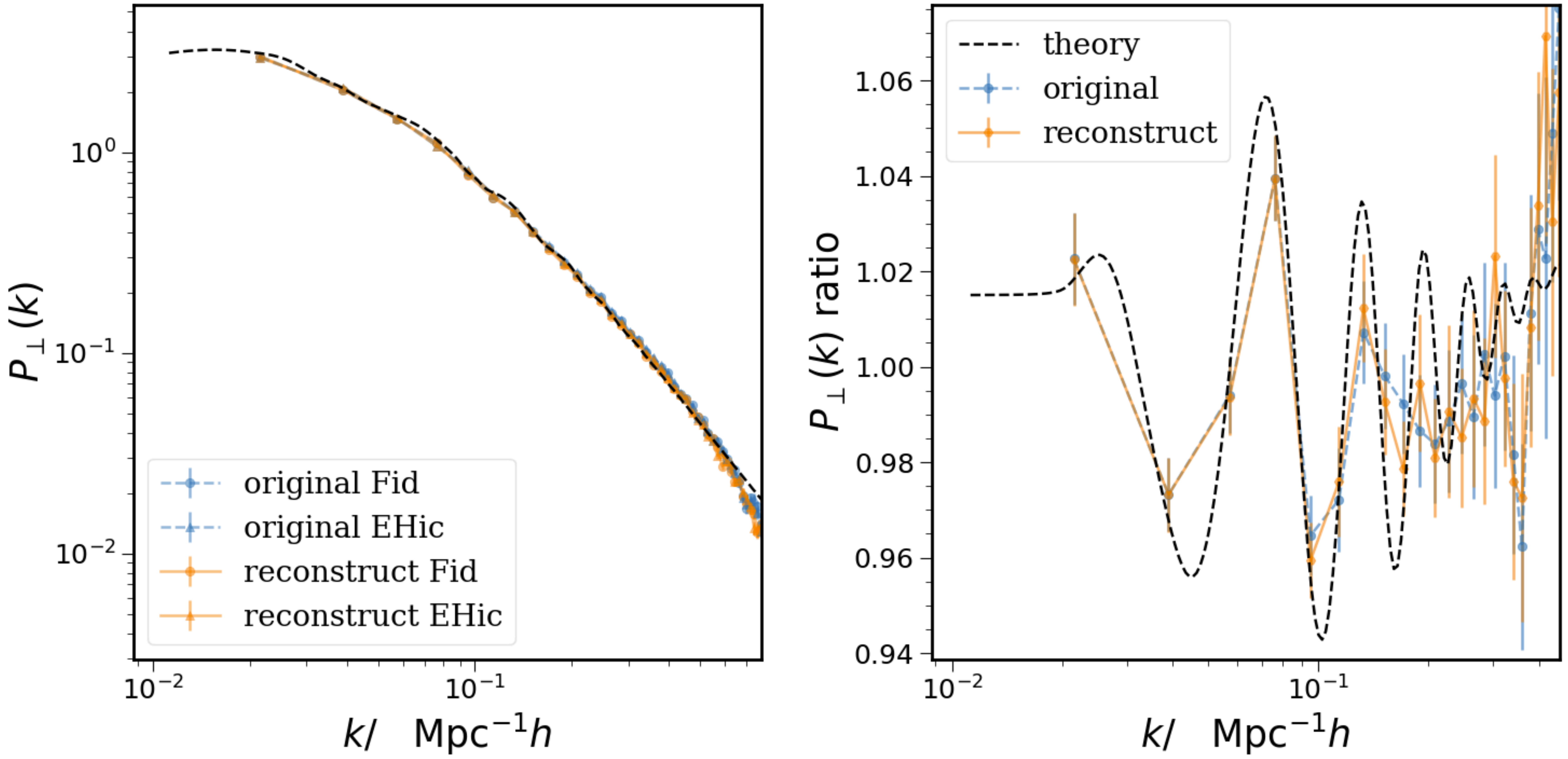

Prospects of application to survey data

- Transverse BAO reconstruction can enhance the BAO signals in the data.
- The simple ZA reconstruction strategy can be easily applied to survey data
- BAO reconstruction relies on the number density of the sample (the actual BAO sample number density is much higher than the halo number density here)
- Plan to apply to DES Y6 data.

Conclusions

- DES Y3 uses w and Cl to derive the tightest BAO constraints from photometric data.
- Using DES Y3 data, we apply the 3D correlation function to measure the BAO. The results are consistent with angular correlation analyses. The deviation from Planck is reduced from 2.5 sigma (w) to 1.6 sigma (ξ_p).
- ξ_p is complementary to the angular statistics, serve as useful crosscheck, one of the fiducial statistics in Y6 BAO analysis.
- BAO reconstruction can be applied to photometric data to enhance the BAO significance